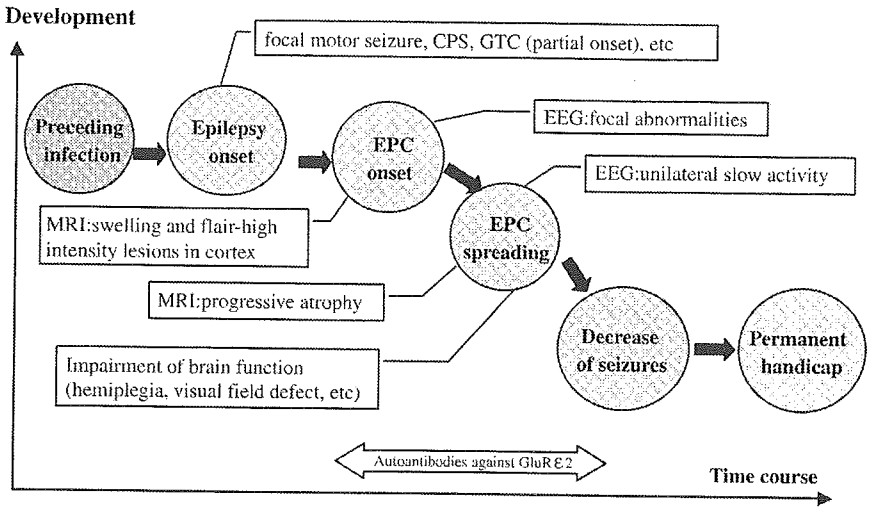

Figure 1. Schematic presentation of the typical clinical course of Rasmussen syndrome. After preceding infections, epileptic seizures (focal motor seizures or partial onset generalized tonic clonic convulsions, etc.) appear, followed by progressive deterioration of clinical symptoms and aggravation of EEGs and MRI abnormalities. In the residual stage, permanent handicap is observed, but epileptic seizures decrease. GTC, generalized tonic clonic seizure; GluR, glutamate receptor; EPC, epilepsia partialis continua.

unavoidable after operation. When the dominant side is affected, there is no effective therapy.

Viral infections were implicated as the causal agent of Rasmussen's encephalitis in early investigations (Andermann 1991), and direct infection by several candidate viruses (CMV, tick-borne encephalitis virus, etc.) has been postulated as one of the possible mechanisms causing the disease (Takahashi 2006) (Figure 2).

Rogers et al. (1994) reported glutamate receptor 3 (GluR3) as an autoantigen in Rasmussen's encephalitis, and proposed autoantibodies against this molecule to be one cause of Rasmussen's encephalitis (humoral autoimmune hypothesis). Their report

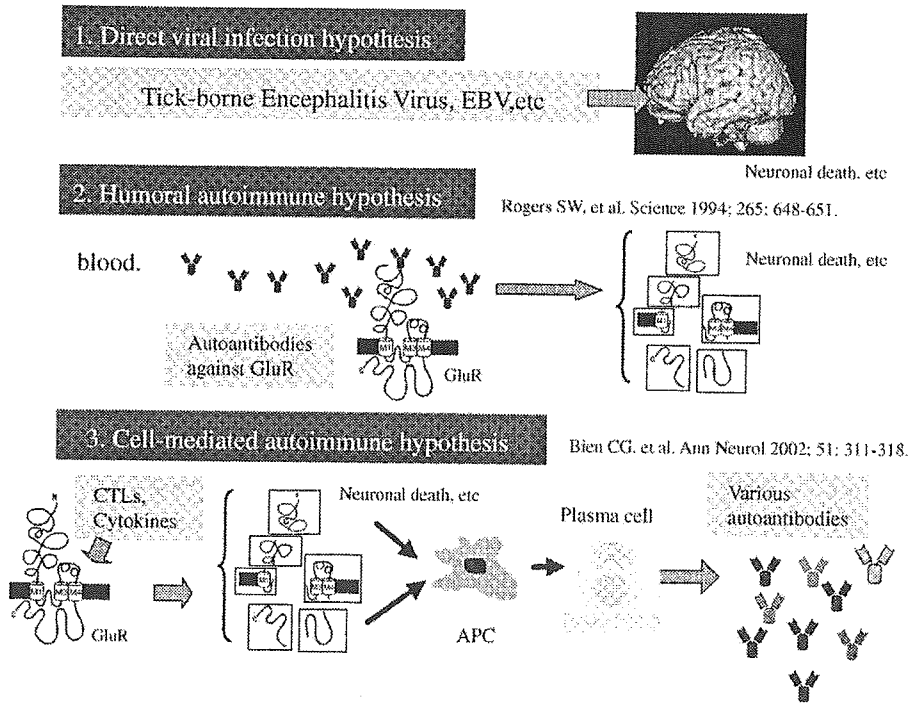

Figure 2. Hypotheses of autoimmune pathologies in Rasmussen syndrome. Direct viral infection hypothesis presumes that viral particles invade the brain and cause neuronal death, etc. Humoral autoimmune hypothesis supposes that autoantibodies against neural molecules (GluR3, etc.) play the primary roles to develop Rasmussen syndrome. Cell-mediated autoimmune hypothesis speculates that CTLs and/or cytokines from $CD4^{+}$T cells play the primary roles. EBV, Ebstein bar virus; GluR, glutamate receptor; APC, antigen-presenting cells.

introduced a new perspective of autoimmune-mediated mechanism to the field of epilepsy. Several pathological roles of autoantibodies against GluR3 have been demonstrated, including excitotoxicity (Levite and Hermelin 1999), complement-dependent cell death (He et al. 1998) and membrane attack complex (MAC) (Xiong and McNamara 2002, Xiong et al. 2003) have been shown, although induction of currents through GluR remains controversial (Twyman et al. 1995, Watson et al. 2004). The MAC is composed of several complements, and appears to induce functional pore in cell membrane, leading to depolarization and osmotic lysis of neurons. These data indicate that autoantibodies can directly cause impairment of neural functions.

On the other hand, Bien et al. (2002a) proposed the destruction of neurons by cytotoxic T cells (CTLs) as a new pathogenic mechanism in Rasmussen's encephalitis (cell-mediated autoimmune hypothesis). Lymphocytic infiltration containing predominantly T cells and sparsely B cells can be observed in surgically resected tissues from patients with Rasmussen's encephalitis (Farrell et al. 1995), and local CNS immune responses in Rasmussen's encephalitis include clonal expansion of T cells responding to discrete antigen epitopes (Li et al. 1997). Peripheral blood lymphocytes from patients are sensitized to GluRε2 (Takahashi et al. 2005). Heterogeneous autoantibodies against neuronal molecules (including GluR3, GluRε2, neuronal acetylcholine receptor alpha7, and munc-18) (Yang et al. 2000, Watson et al. 2001, Takahashi et al. 2003) and glial cells (Roubertie et al. 2005) are detected in Rasmussen syndrome. Autoantibodies against GluRε2 have epitopes predominantly in intracellular domains, and show epitope spreading evolutionally (Takahashi et al. 2003). We postulate that the autoimmune-mediated mechanism for the development of Rasmussen syndrome involves primarily cellular autoimmunity mediated by cytotoxic T cells, and evolutionarily involves humoral autoimmunity mediated by auto-antibodies (Takahashi et al. 2003, 2005). These autoimmune mechanisms of epileptogenesis after infections can be classified as parainfectious mechanisms (Figure 3) (Takahashi 2006).

Causative factors of in patients with Rasmussen syndrome

In our epilepsy center, 44% of Japanese patients with Rasmussen syndrome had prior infections or vaccinations, and approximately 8% had head trauma as preceding causative factors, and the frequencies are almost same in patients with EPC and in those without EPC (Table I) (Takahashi 2006). The microbes causing infections were not identified in the majority of patients, except in three patients infected by influenza virus and one patient by mycoplasma. Likewise, in the study conducted at Montreal Neurological Institute, the causative microbes were not documented except measles (encephalitis) and varicella (Andermann 1991).

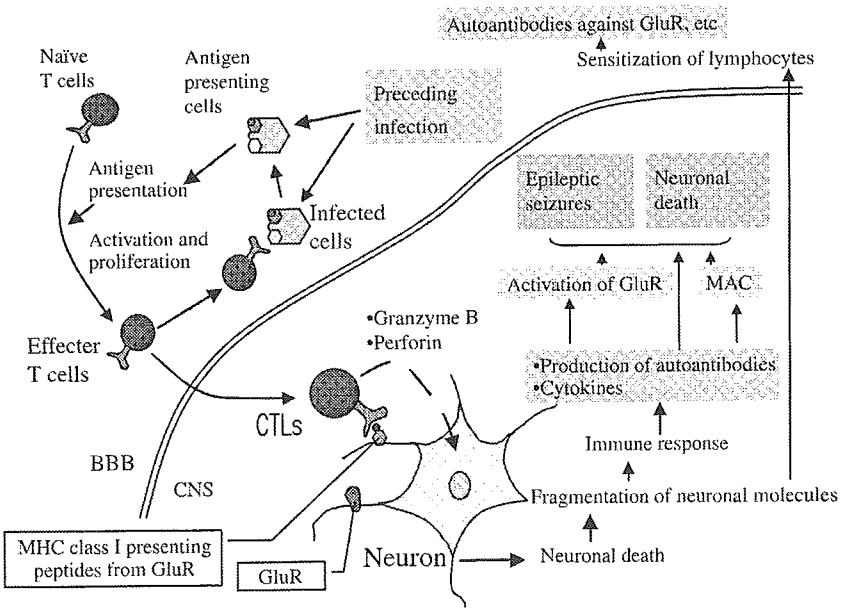

Figure 3. Involvements of CTLs and autoantibodies in the hypothetic mechanisms of the development of Rasmussen syndrome. Effecter T cells activated by preceding infections or vaccinations reach the CNS by crossing blood brain barrier, and cross-react with neurons, etc. resulting in apoptosis. Neuronal death leads to production of autoantibodies against CNS molecules and cytokines, which might contribute to the further neuronal death or epileptogenesis. Fragmented neuronal molecules reach systemic circulation and sensitize lymphocytes, resulting in production of autoantibodies in the blood. BBB, blood brain barrier; CNS, central nervous system; CTLs, cytotoxic T cells; GluR, glutamate receptor; MAC, membrane attack complex.

Table I. Causative factors in 34 patients with Rasmussen syndrome.

	EPC type	Non-EPC type	Total
Age of onset	6.3 ± 5.6	8.7 ± 8.0	7.4 ± 6.7
Preceding infections	8 (40.0%)	5 (35.7%)	13 (38.2%)
Fever only	4	1	5
Upper respiratory infection	2	1	3
Influenza	1	2	3
Mycoplasma	0	1	1
Aseptic meningitis	1	0	1
Vaccination	1 (5.0%)	1 (7.1%)	2 (5.9%)
Head trauma	2 (10.0%)	1 (7.1%)	3 (8.8%)
None	9 (45.0%)	7(50.0%)	16(47.1%)
Total	20	14	34

Therefore, it remains unknown whether specific microbes are involved in the development of Rasmussen syndrome. The contribution of molecular mimicry between microbial and neuronal molecules and degeneracy of T cell receptor recognition to the development of Rasmussen syndrome (autoimmune-mediated epilepsies) will be discussed later.

We encountered two patients who developed Rasmussen syndrome after vaccination, although vaccination was not reported as a causative factor in the series of Montreal Neurological Institute. One patient had EPC type Rasmussen syndrome. This patient received Japanese encephalitis vaccination at the age of 15 years. Two months after vaccination, he had the initial epileptic seizure, and subsequently evolved to intractable and frequent complex partial seizures (CPSs) and EPC. MRI lesions in left frontal lobe and autoantibodies against GluRε2 were detected. Focal resection of the left frontal lobe failed to control epileptic seizures, psychiatric symptoms and deterioration. Another patient had non-EPC type Rasmussen syndrome. This patient received measles–mumps–rubella triple vaccine at the age of 1 year. Three weeks later, he was affected by aseptic meningitis caused by the vaccination. He had intractable epileptic seizures from the age of two, and psychiatric symptoms (including anxiety) evolved subsequently. At the age of 14 years, right frontal lobectomy was conduced and successfully controlled the seizures.

Head trauma also was not reported as a causative factor in the patients of Montreal Neurological Institute, but we identified three patients with Rasmussen syndrome possibly related to preceding head trauma. As we sometimes experience patients with aseptic meningitis after head trauma, head trauma may facilitate the invasion of inflammatory T cells into the CNS. In patients with post-concussion syndrome after mild head injury, focal cortical dysfunction may occur in conjunction with the disruption of the blood brain barrier (Korn et al. 2005).

In the following sections, infection as a causative factor in Rasmussen syndrome will be illustrated using a specific case in which Rasmussen syndrome developed after influenza infection, especially focusing on the roles of molecular mimicry and HLA class I.

A case of Rasmussen syndrome after influenza A infection, and cross-reaction of lymphocytes

This patient, a boy, was 8 year-old at the time of this report (Case 1). His family history was unremarkable, with ovarian cyst in his mother and parkinsonism in his maternal grandfather. At the age of 3 years and 11 months, he had febrile generalized convulsion following an episode of influenza A infection that was confirmed by antigen detection from a nasal sample. Before the influenza infection, he had no neurological symptoms and no other preceding conditions that might precipitate the convulsions. Soon after the initial convulsion, at age 4, he had febrile convulsive status of left extremities associated with repeated influenza A infection. CSF was normal, and CT revealed no abnormalities. At the age of 4 years and 1 month, afebrile convulsive status appeared and phenobarbital (50 mg) was prescribed. Thereafter, his seizures became progressively intractable, in spite of a combination of several antiepileptic drugs (carbamazepine, zonisamide, valproic acid and phenytoin). At the age of 5 years and 4 months, EPC appeared after phenytoin was stopped abruptly and clobazam was added. He was referred to our epilepsy center for the treatment of Rasmussen syndrome at the age of 5 years and 5 months. He had hemiparesis of left extremities, EPC of left lower extremity, and several partial seizures in a day (Figure 4). After functional hemispherectomy, seizures were controlled completely. At age eight, he walked to school and attended a normal elementary school.

At presentation, IgG-autoantibodies against GluRε2 were detected in serum and CSF samples (Takahashi et al. 2003), but IgM-autoantibody was negative. The stimulation index obtained in the lymphocyte stimulation test (LST) stimulated with homogenates containing GluRε2 (^{3}H-thymidine

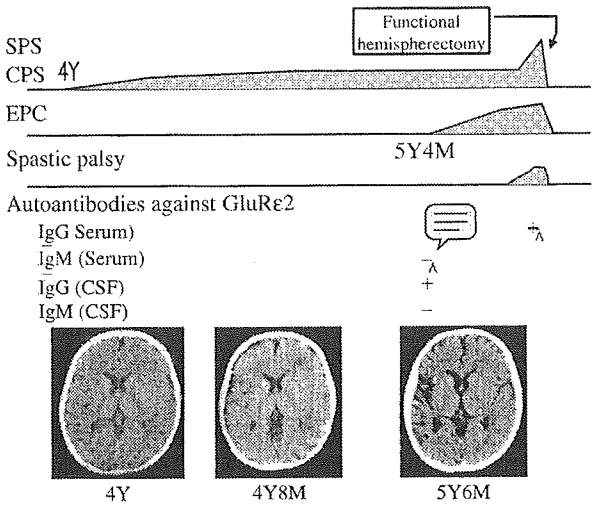

Figure 4. Clinical course of Case 1. Epilepsy occurred at the age of four, and progressive atrophy of right hemisphere started at the age of 5 year and 6 months. IgG-autoantibodies against GluRε2 were positive on admission, but became negative after functional hemispherectomy that successfully controlled seizures. SPS, simple partial seizure; CPS, complex partial seizure; EPC, epilepsia partialis continua.

uptake with stimulation/control ^{3}H-thymidine uptake) was 2.78 (Takahashi et al. 2005), and was higher than normal controls (0.63, 1.67) tested simultaneously (Figure 5). When LST was conducted by co-stimulation with homogenates containing GluRε2 and influenza vaccine, the stimulation index was 9.19 in this patient (Case 1 in Figure 5), and was

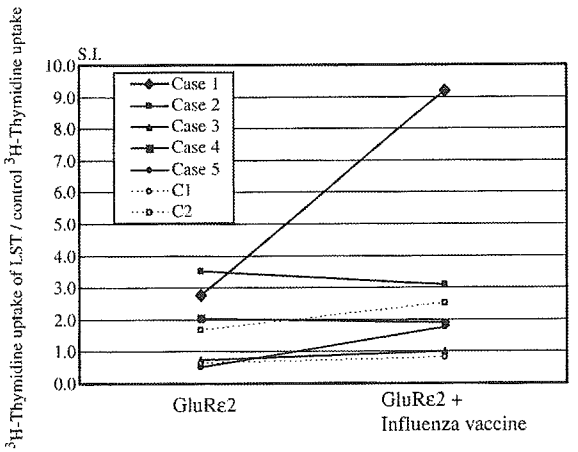

Figure 5. Stimulation index in lymphocyte stimulation test. Data on the left show stimulation indices (SI) (^{3}H-thymidine uptake with stimulation/control ^{3}H-thymidine uptake) obtained in lymphocyte stimulation test (LST) stimulated with homogenate containing GluRε2 (Takahashi et al. 2005). Data on the right show SI when LST was conducted by co-stimulation with homogenates containing GluRε2 and influenza vaccine. Case 1 is the case presented in the text, with influenza A infection as a causative factor. Case 2 is Rasmussen syndrome with no causal relationship with influenza. Cases 3–5 are epileptic cases (no Rasmussen syndrome) with autoantibodies against GluRε2. C1 and C2 are normal controls.

higher compared with other patients with Rasmussen syndrome or other epilepsies not related to preceding influenza infection (Cases 2–5). A synergistic increase in stimulation index with co-stimulation (GluRε2 + influenza vaccine) compared to GluRε2 stimulation alone was observed only in the present case. These data suggest that the lymphocytes of this patient are sensitized not only by influenza antigen but also by GluRε2, and that the T cell receptors of this patient can cross-react with peptides from influenza and GluRε2.

After the T cell receptors on CTLs recognize both the HLA class I molecule and its binding peptide expressed on antigen presenting cells (APCs), these CTLs are activated into cytotoxic effector cells that are capable of invading the CNS. If through molecular mimicry and T cell receptor redundancy, the CTLs activated by microbial peptides are able to recognize the HLA class I and binding peptide expressed on neurons, then the infection-activated CTLs may induce apoptosis of neurons. Therefore, HLA class I is one of the key molecules that determines autoimmune mechanisms underlying the process leading from infection or vaccination to Rasmussen syndrome.

HLA class I and theoretical cross-reaction of CTLs in Case 1

In the case presented above (Case 1), HLA genotyping identified HLA − A*0201, A*2402, and B*3501 (homo). HLA − A*0201 binds peptides with the following motif: [LM] − x(3) − V − x(2) − [VL] (x, free amino acid; L, leucine; M, methionine; V, valine). Database analyses (Genome Net: http://www.genome.jp/) revealed this motif in various viral molecules and neural molecules (Figure 6). If patients with HLA − A*0201 are infected by influenza A virus, the peptide *LAIMVAGL* from the hemagglutinin of influenza A is able to bind with A*0201 expressed on APCs. CTLs with T cell receptors that recognize A*0201 and the hemagglutinin peptide (influenza A) on APCs become activated and become effector CTLs. Theoretically, these effector CTLs can invade the CNS, and react with neurons expressing HLA − A*0201 and peptides containing the [LM] − x(3) − V − x(2) − [VL] motif, due to molecular mimicry and degeneracy of T cell receptor recognition (Uemura et al. 2003). Peptides having the HLA − A*0202 binding motif are found in various neuronal molecules, such as GluRε2 (*LVLAVLAV*, *MLLIVSAV*) and GluRε1 (*L*PLD*V*NV*V*). Therefore, we hypothesize that CTLs activated by influenza may cross-react with neurons that express GluRε2 under specific conditions such as the presence of costimulators. This hypothetic cross-reaction based on molecular mimicry of HLA-binding motif is compatible with our data of

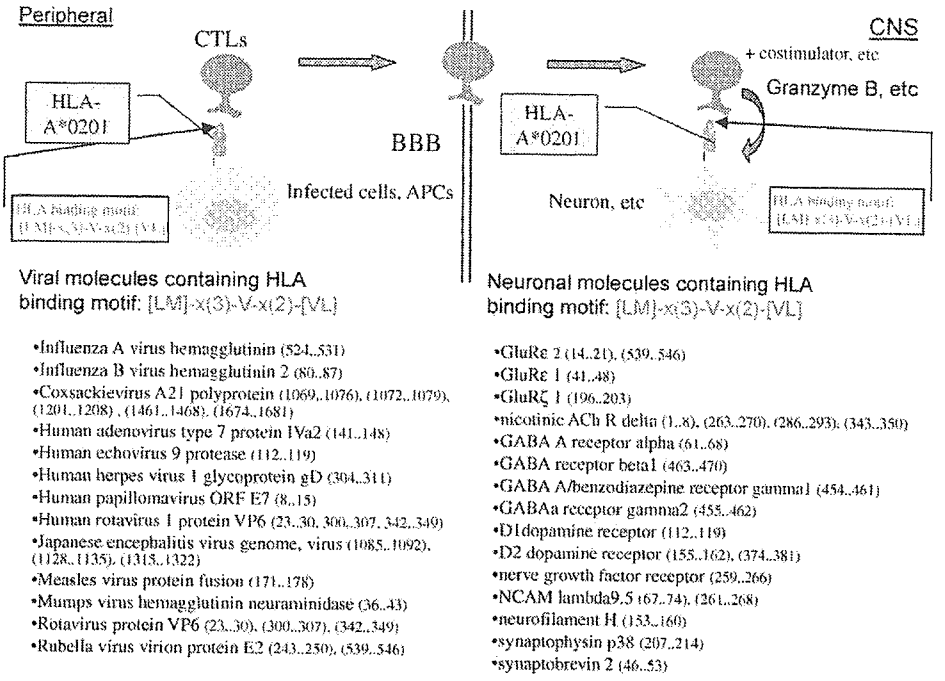

Figure 6. Viral and neural molecules containing specific binding motif for HLA − A*0201. Viral infection of host cells leads to expression of some parts of the viral peptides by binding with HLA class I molecule on the infected cells. CTLs expressing T cell receptors that recognize the peptide and HLA class I are activated, resulting in generation of effecter T cells. In individuals with HLA − A*0201, the binding motif is [LM] − $x(3)$ − V − $x(2)$ − [VL] (x, free amino acid; L, leucine; M, methionine; V, valine). Database analyses (Genome Net, http://www.genome.jp/) revealed many viral molecules containing this motif, as shown in the left column. The numbers in parentheses are sequence numbers indicating the sites of the motif. Effecter T cells are able to cross the blood brain barrier to reach the CNS, and theoretically can cross-react with neurons expressing the same motif on HLA class I, under specific conditions such as the presence of costimulator. Database analyses revealed many neural molecules including NMDA-GluRs, which contain the motif, as shown in the right column.

lymphocyte cross-reactivity between GluRε2 and influenza vaccine observed in Case 1 (Figure 5). Since CTLs activated by influenza can react with a broad spectrum of neuronal molecules, theoretically, apoptotic lesions caused by CTLs may distribute widely in the brain. On the other hand, possible interactions of the activated CTLs of Case 1 with a variety of microbial molecules (Figure 6) may explain the symptomatic aggravation triggered by infections other than influenza after the onset of Rasmussen syndrome. T cell clones from type 1 diabetes patients have been shown to react with several kinds of microbial mimicry peptides (Uemura et al. 2003). Similar molecular mimicry may also exists for HLA − A*2402 and B*3501. These molecules also have specific binding motifs. Database search identified diverse peptides containing these specific motifs in both microbial and neural molecules.

HLA class I in patients with Rasmussen syndrome

We studied the genotypes of HLA class I in 16 Japanese patients with Rasmussen syndrome (EPC type, 9; non-EPC type, 7) by PCR amplifications. The data were analyzed statistically using Chi-square for independence test. HLA − A*2402 is a popular genotype (36.5% of Japanese population) and was found in 77.8% of EPC type patients ($p = 0.016$). The frequencies of HLA − A*0201 and HLA − A*2601 were higher in non-EPC type patients (both 42.9%) than in Japanese population (10.7 and 11.3%, respectively) ($p = 0.033$ and 0.038, respectively). HLA − B*5201was found more frequently in EPC type patients (33.3%) than in Japanese population (10.9%) ($p = 0.070$), while HLA − B*4601 was more frequent in non-EPC type patients (28.6%) than in Japanese population (3.4%) ($p = 0.025$). The relative risks of various HLA class I genotypes for Rasmussen syndrome range from 6 to 11 (Table II), which are at the same levels as systemic lupus erythematosus (DR2) and acute anterior uveitis (B27) (Marsh et al. 2000). The relative risks of HLA class I-A and B haplotypes range from 5 to ∞. Since the haplotype of A*2601 + B*5401 was not observed in 561 Japanese subjects, the risk is infinity.

The HLA class I types that have higher relative risks may have a greater potential to induce cross-reactions of CTLs between microbes and neurons, and consequently may be found at higher frequencies in patients with Rasmussen syndrome. The binding motifs of these HLA class I types probably exist frequently in molecules from microbes commonly found in Japan and in molecules derived from neurons.

Table II. HLA class I genotypes and relative risks in patients with Rasmussen syndrome.

HLA genotypes	Clinical phenotype	Relative risk
HLA class I-A		
A*2402	EPC type	6.1
A*0201	Non-EPC type	6.4
A*2601	Non-EPC type	6.3
HLA class I-B		
B*4601	Non-EPC type	11.4
HLA – A + B haplotypes		
A*2402 + B*4801	EPC type	13.3
A*2402 + B*1501	EPC type	21.1
A*2402 + B*5201	EPC type	5.1
A*2601 + B*5401	Non-EPC type	∞

∞, infinity.

Acknowledgements

The author thanks Masayoshi Mishina and Hisashi Mori for their helpful comments, and Shigeko Nishimura and Hisano Tsunogae for their skillful assistance. This study was funded in part by Research Grants (16A-3) for Nervous and Mental Disorders from the Ministry of Health, Labor and Welfare, grants-in-aid for Scientific Research I No. 15591151, 16590859, and 17591133, Health and Labour Sciences Research Grants for Research on Psychiatry and Neurological Diseases and Mental Health (H17-017) and Research on Children and Families (H16-016), and grants from The Japan Epilepsy Research Foundation.

References

Aguilar MJ, Rasmussen T. 1960. Role of encephalitis in pathogenesis of epilepsy. AMA Arch Neurol 2:663–676.

Andermann F, editor. 1991. Chronic encephalitis and epilepsy: Rasmussen's syndrome. Boston: Butterworth-Heinemann.

Bien CG, Bauer J, Deckwerth TL, et al. 2002a. Destruction of neurons by cytotoxic T cells: A new pathogenic mechanism in Rasmussen's encephalitis. Ann Neurol 51:311–318.

Bien CG, Widman G, Urbach H, et al. 2002b. The natural history of Rasmussen's encephalitis. Brain 125:1751–1759.

Farrell MA, Droogan O, Secor DL, Poukens V, Quinn B, Vinters HV. 1995. Chronic encephalitis associated with epilepsy: Immunohistochemical and ultrastructural studies. Acta Neuropathol 89:313–321.

He XP, Patel M, Whitney KD, Janumpalli S, Tenner A, McNamara JO. 1998. Glutamate receptor GluR3 antibodies and death of cortical cells. Neuron 20:153–163.

Korn A, Golan H, Melamed I, Pascual-Marqui R, Friedman AJ. 2005. Focal cortical dysfunction and blood–brain barrier disruption in patients with Postconcussion syndrome. Clin Neurophysiol 22:1–9.

Levite M, Hermelin A. 1999. Autoimmunity to the glutamate receptor in mice—a model for Rasmussen's encephalitis? J Autoimmun 13:73–82.

Li Y, Uccelli A, Laxer KD, et al. 1997. Local-clonal expansion of infiltrating T lymphocytes in chronic encephalitis of Rasmussen. J Immunol 158:1428–1437.

Marsh SGE, Parham P, Barber LD. 2000. The HLA factsBook. London: Academic Press. p 79–83.

Rogers SW, Andrews PI, Gahring LC, et al. 1994. Autoantibodies to glutamate receptor GluR3 in Rasmussen's encephalitis. Science 265:648–651.

Roubertie A, Boukhaddaoui H, Sieso V, et al. 2005. Antiglial cell autoantibodies and childhood epilepsy: A case report. Epilepsia 46:1308–1312.

Takahashi Y. 2006. Vaccination and infection as causative factors of epilepsy. Future Neurol (in press).

Takahashi Y, Mori H, Mishina M, et al. 2003. Autoantibodies to NMDA receptor in patients with chronic forms of epilepsia partialis continua. Neurology 61:891–896.

Takahashi Y, Mori H, Mishina M, et al. 2005. Autoantibodies and cell-mediated autoimmunity to NMDA-type GluRε2 in patients with Rasmussen's encephalitis and chronic progressive epilepsia partialis continua. Epilepsia 46(Suppl 5):152–158.

Twyman RE, Gahring LC, Spiess J, Rogers SW. 1995. Glutamate receptor antibodies activate a subset of receptors and reveal an agonist binding site. Neuron 14:755–762.

Uemura Y, Senju S, Maenaka K, et al. 2003. Systematic analysis of the combinatorial nature of epitopes recognized by TCR leads to identification of mimicry epitopes for glutamic acid decarboxylase 65-specific TCRs. J Immunol 170:947–960.

Watson R, Jiang Y, Bermudez I, et al. 2004. Absence of antibodies to glutamate receptor type 3 (GluR3) in Rasmussen encephalitis. Neurology 63:43–50.

Watson R, Lang B, Bermudez I, et al. 2001. Autoantibodies in Rasmussen's encephalitis. J Neuroimmunol 118:148.

Xiong ZO, McNamara JO. 2002. Fleeting activation of ionotropic glutamate receptors sensitizes cortical neurons to complement attack. Neuron 36:363–374.

Xiong ZO, Qian W, Suzuki K, McNamara JO. 2003. Formation of complement membrane attack complex in mammalian cerebral cortex evokes seizures and neurodegeneration. J Neurosci 23: 955–960.

Yang R, Puranam RS, Butler LS, et al. 2000. Autoimmunity to munc-18 in Rasmussen's encephalitis. Neuron 28:375–383.

Development/Plasticity/Repair

Control of Synaptic Connection by Glutamate Receptor δ2 in the Adult Cerebellum

Tomonori Takeuchi,[1]* Taisuke Miyazaki,[2]* Masahiko Watanabe,[2] Hisashi Mori,[1] Kenji Sakimura,[3] and Masayoshi Mishina[1]

[1]Department of Molecular Neurobiology and Pharmacology, Graduate School of Medicine, University of Tokyo, and Solution Oriented Research for Science and Technology, Japan Science and Technology Agency, Tokyo 113-0033, Japan, [2]Department of Anatomy, Hokkaido University School of Medicine, Sapporo 060-8638, Japan, and [3]Department of Cellular Neurobiology, Brain Research Institute, Niigata University, Niigata 951-8585, Japan

Precise topological matching of presynaptic and postsynaptic specializations is essential for efficient synaptic transmission. Furthermore, synaptic connections are subjected to rearrangements throughout life. Here we examined the role of glutamate receptor (GluR) δ2 in the adult brain by inducible and cerebellar Purkinje cell (PC)-specific gene targeting under the pure C57BL/6 genetic background. Concomitant with the decrease of postsynaptic GluRδ2 proteins, presynaptic active zones shrank progressively and postsynaptic density (PSD) expanded, resulting in mismatching between presynaptic and postsynaptic specializations at parallel fiber–PC synapses. Furthermore, GluRδ2 and PSD-93 proteins were concentrated at the contacted portion of mismatched synapses, whereas AMPA receptors were distributed in both the contacted and dissociated portions. When GluRδ2 proteins were diminished, PC spines lost their synaptic contacts. We thus identified postsynaptic GluRδ2 as a key regulator of the presynaptic active zone and PSD organization at parallel fiber–PC synapses in the adult brain.

Key words: cerebellar Purkinje cell; conditional gene targeting; glutamate receptor δ2; postsynaptic density; synaptic connection; synaptic matching

Introduction

Brain function is based on highly complex neural networks and their dynamics. Efficient synaptic transmission requires elaborate structural specializations in both presynaptic and postsynaptic cells and precise topological matching of presynaptic transmitter release machineries and postsynaptic neurotransmitter receptor complexes. Furthermore, changes in spine morphology and number after learning are observed in several brain regions, including the cerebellum (Bailey and Kandel, 1993; Lamprecht and LeDoux, 2004). Although molecular understanding of synapse formation during development is emerging (Hering and Sheng, 2001; Goda and Davis, 2003; Scheiffele, 2003), the molecular mechanism for regulation of synaptic connections in the adult brain remains to be investigated.

The δ subfamily of glutamate receptor (GluR) was found by molecular cloning (Yamazaki et al., 1992), and it positions in between the classical AMPA–kainate and NMDA subtypes from the amino acid sequence identity. GluRδ2, the second member of this subfamily, is selectively expressed in cerebellar Purkinje cells (PCs) (Araki et al., 1993; Lomeli et al., 1993), and within PCs, GluRδ2 proteins are localized exclusively at parallel fiber (PF)–PC synapses (Takayama et al., 1996; Landsend et al., 1997). Our previous studies showed that mutant mice lacking GluRδ2 are defective in long-term depression at PF–PC synapses, motor learning, and motor coordination (Funabiki et al., 1995; Kashiwabuchi et al., 1995; Kishimoto et al., 2001; Mishina, 2003). In addition, the number of PF–PC synapses decreased and innervation of PCs by multiple climbing fibers was sustained in GluRδ2 mutant mice (Kashiwabuchi et al., 1995; Kurihara et al., 1997; Hashimoto et al., 2001; Lalouette et al., 2001; Ichikawa et al., 2002). These studies revealed that in cerebellar PCs, in which functional NMDA receptors are absent, GluRδ2 plays a central role in synaptic plasticity, motor learning, and cerebellar wiring. However, the primary role of GluRδ2 and whether GluRδ2 regulates synaptic connections in the adult brain or only during development remained to be investigated. The NMDA receptor also plays important roles both in learning and memory (Martin et al., 2000) and in neural network formation during development (Goodman and Shatz, 1993). Furthermore, activation of NMDA receptors induces structural alterations of spines of cultured hippocampal neurons (Engert and Bonhoeffer, 1999; Maletic-Savatic et al., 1999). On the other hand, ablation of NMDA receptors in the adult brain exerted no detectable effects on synaptic structures (Tsien et al., 1996; Rampon et al., 2000).

Received Nov. 19, 2004; revised Jan. 11, 2005; accepted Jan. 12, 2005.

This work was supported in part by research grants from the Ministry of Education, Culture, Sports, Science, and Technology of Japan and the Japan Science and Technology Agency. We thank R. Natsume for chimeric mouse preparation, C. Stewart for ES cells, T. Yagi for plasmid pMC1DTpA, T. Ogura, K. Yoshitake, and T. Yamaguchi for help in mouse breeding, and Y. Nakajima for help in the preparation of this manuscript. We are grateful to M. Ohtsuka for his encouragement and support.

*T.T. and T.M. contributed equally to this work.

Correspondence should be addressed to Masayoshi Mishina, Department of Molecular Neurobiology and Pharmacology, Graduate School of Medicine, University of Tokyo, Tokyo 113-0033, Japan. E-mail: mishina@m.u-tokyo.ac.jp.

H. Mori's present address: Department of Molecular Neuroscience, Graduate School of Medicine, Toyama Medical and Pharmaceutical University, Toyama 930-0194, Japan.

DOI:10.1523/JNEUROSCI.4740-04.2005

 0270-6474/05/252146-11$15.00/0

Thus, it is crucial to determine whether the diverse functional roles of GluRδ2 revealed by studies of conventional knock-out mice, especially regulation of cerebellar wiring, are specific for the developmental stage, although we suggested a close relationship in the molecular mechanism between synaptic plasticity at the adult stage and synapse formation during development in the cerebellum (Kashiwabuchi et al., 1995). To address this issue, we generated a target mouse line carrying the *GluRδ2* gene flanked by *loxP* sequences using embryonic stem (ES) cells derived from the C57BL/6 strain. Crossing the target mouse with a Cre mouse line carrying the Cre recombinase–progesterone receptor fusion protein (CrePR) gene under the control of the *GluRδ2* gene promoter enabled us to inductively abolish GluRδ2 proteins selectively in cerebellar PCs of the mature brain. Here we report the effects of inducible ablation of GluRδ2 proteins on the structures of PF–PC synapses in the adult cerebellum.

Materials and Methods

Generation of mice. We isolated a mouse genomic clone carrying exon 12 of the *GluRδ2* gene by screening a bacterial artificial chromosome library prepared from the C57BL/6 strain (Incyte Genomics, St. Louis, MO) using a mouse *GluRδ2* cDNA encoding putative transmembrane segments M1–M3 as a probe. The 7.9 kb *Bam*HI fragment from the genomic clone was subcloned into the *Bam*HI site of pBluescript II KS(+) (Stratagene, La Jolla, CA) to yield pGRD2B1. The 1.8 kb DNA fragment carrying the 34 bp *loxP* sequence and *Pgk-1* promoter-driven neomycin phosphotransferase gene (*neo*) flanked by two Flp recognition target (*frt*) sites was inserted into the *Hin*cII site 381 bp upstream of exon 12, and the 34 bp *loxP* sequence with 10 bp linker sequences into the *Hin*dIII site 122 bp downstream of exon 12. The targeting vector pTVD2V4 contained exon 12 of the *GluRδ2* gene flanked by *loxP* sequences, the 9.9 kb upstream and 2.3 kb downstream genomic sequences, and 4.3 kb pMC1DTpA (Taniguchi et al., 1997).

We isolated a subclone of ES cells derived from the C57BL/6 strain (Köntgen et al., 1993). ES cells were cultured on mitomycin C-treated neomycin-resistant fibroblasts in knock-out DMEM supplemented with 17.9% knock-out serum replacement (Invitrogen, Carlsbad, CA), 90.7 μM nonessential amino acids, 1 mM L-glutamine, 100 μM 2-mercaptoethanol, and 1×10^3 U/ml leukemia inhibitory factor (Chemicon International, Temecula, CA) at 37°C under humidified atmosphere containing 5% CO_2. The targeting vector was linearized by *Not*I and electroporated into ES cells using Gene Pulser (Bio-Rad, Hercules, CA) (250 V, 960 μF, $r = \infty$). G-418 selection (150 μg/ml) was started 36–48 h after electroporation and continued for 1 week. Recombinant clones were identified by Southern blot hybridization analysis of *Sca*I- or *Nhe*I-digested genomic DNA using the 0.6 kb *Eco*81I–*Msc*I fragment from pGRD2B1, the 0.6 kb *Pst*I fragment from pLFNeo (Takeuchi et al., 2002), and the 4.0 kb *Hin*dII–*Nhe*I fragment from pD2–9 (Kashiwabuchi et al., 1995) as 5′, neo, and 3′ probes, respectively. Recombinant ES cells were injected into eight-cell stage embryos of ICR mice. The embryos were cultured to blastocysts and transferred to the pseudopregnant ICR uterus.

Resulting chimeric mice were mated to FLP66 transgenic mice of the C57BL/6 strain (Takeuchi et al., 2002), and male offspring were further crossed with C57BL/6 mice. Elimination of the *neo* gene from the genome through Flp/frt-mediated excision was identified by Southern blot hybridization analysis with a 3′ probe. *GluRδ2*$^{+/flox}$ mice were crossed with *GluRδ2*$^{+/CrePR}$ mice (Kitayama et al., 2001) to yield *GluRδ2*$^{flox/CrePR}$ mice. Littermates derived from crossing of *GluRδ2*$^{flox/flox}$ and *GluRδ2*$^{flox/CrePR}$ mice with the pure C57BL/6 genetic background were used for subsequent studies. Animal care was performed in accordance with institutional guidelines. Mice were fed *ad libitum* with standard laboratory chow and water in standard animal cages under a 12 h light/dark cycle.

The *GluRδ2*^{flox} allele was identified by PCR using primers 5′-AGCAACCTACACTCCCAAAGAAG-3′ (FD2P3) and 5′-ATTCAGTGCCAAGACAGACAACAA-3′ (FD2P4) or by Southern blot hybridization analysis of *Nhe*I-digested genomic DNA with a 3′ probe. The *GluRδ2*^{CrePR} allele was identified by PCR using CreP1 and CreP2 primers (Tsujita et al., 1999).

Induction of recombination. RU-486 (Sigma, St. Louis, MO) was suspended at a concentration of 50 mg/ml in water containing 0.25% (v/v) carboxymethyl cellulose and 0.5% (v/v) Tween 80. We injected 1 mg/g body weight of RU-486 into the peritoneum of *GluRδ2*$^{flox/flox}$ and *GluRδ2*$^{flox/CrePR}$ mice at postnatal day 42 (P42)–P45 for 2 consecutive days. *In situ* hybridization analysis of *GluRδ2* mRNA was performed as described (Watanabe et al., 1993) using oligonucleotide probes 5′-ACCAAGCCCCCATCATCATTCGGGTTGCCAGAGTTGTGTATGGGA-3′ and 5′-CTCTCAATGCGGGTGATAGTGAGGAAAGCGGCAAGGTTGGCTGTA-3′ in mixture. Autoradiographic silver grains on PCs and the granular layer were counted to obtain the signal and noise levels, respectively. Quantitative immunoblotting analysis of GluRδ2 proteins in cerebellar homogenate was performed using rabbit anti-GluRδ2 antibody (Araki et al., 1993) and chemiluminescence (Amersham Biosciences, Piscataway, NJ). The images were acquired using a CCD camera (LAS-1000plus; Fuji Photo Film, Tokyo, Japan) and analyzed with Science Lab 98 Image Gauge (Fuji Photo Film). GluRδ2 signals were normalized with those of GluRε1 (Watanabe et al., 1998) as an internal standard.

Histology and immunofluorescence. Under deep pentobarbital anesthesia (100 μg/g of body weight, i.p.), mice were perfused transcardially with 4% paraformaldehyde in 0.1 M sodium phosphate buffer, pH 7.4, and processed for paraffin sections (5 μm) with a sliding microtome (SM2000R; Leica Microsystems, Nussloch, Germany). Paraffin sections were stained with hematoxylin or immunostained with rabbit anti-GluRδ2 antibody (Araki et al., 1993) and guinea pig anti-calbindin antibody (Nakagawa et al., 1998) followed by incubation with species-specific FITC- and Cy3-conjugated secondary antibodies (Jackson ImmunoResearch, West Grove, PA). Photographs were taken by a fluorescence microscope (AX-70; Olympus, Tokyo, Japan) or a confocal laser scanning microscope (Fluoview; Olympus).

Electron microscopy. For qualitative and quantitative analyses by conventional electron microscopy, ultrathin sections cut in the parasagittal plane were prepared from the straight portion of lobules 4/5. Serial ultrathin sections were mounted on formvar-supported copper grids and stained with 2% uranyl acetate for 5 min and mixed lead solution for 2 min. In each mouse, electron micrographs were taken randomly from the neuropil of the molecular layer. Electron micrographs were taken at an original magnification of 4000× or 10,000× using an H-7100 electron microscope (Hitachi High-Technologies, Tokyo, Japan), and printed at a final magnification of 16,000× or 40,000×. For measurement of active zone and postsynaptic density (PSD) lengths, electron micrographs were scanned and analyzed with MetaMorph software (Molecular Devices, Sunnyvale, CA). The two-dimensionally reconstructed images were drawn and processed for smoothing with Adobe Illustrator software (version 10; Adobe Systems, San Jose, CA). For phosphotungstic acid cytochemistry, microslicer sections (300 μm in thickness) were dehydrated in graded alcohols and incubated in 1% phosphotungstic acid in ethanol for 1 h and embedded in Epon812 resin.

Postembedding immunogold. For postembedding immunogold electron microscopy, microslicer sections (300 μm in thickness) were cryoprotected with 30% glycerol in 0.1 M sodium phosphate buffer, pH 7.4, and frozen rapidly in liquid propane in a cryofixation unit (CPC; Leica Microsystems). The specimens were transferred to 0.5% uranyl acetate in methanol in a cryosubstitution unit (AFS; Leica Microsystems) and embedded in Lowicryl HM20 resin (Electron Microscopy Sciences, Hatfield, PA). Serial ultrathin sections were mounted on Formvar-supported nickel grids for GluRδ2 labeling, whereas for PSD-93 and AMPA receptor labeling, single sections were mounted directly to nickel grids. For the single-section labeling, sections were etched with a saturated solution of NaOH in absolute ethanol for a few seconds. After blocking with 2% human serum albumin (Wako Pure Chemicals, Osaka, Japan) in 10 mM Tris-buffered saline, pH 7.6, grids were immunoreacted with rabbit anti-GluRδ2 antibody (20 μg/ml) or rabbit anti-PSD-93 antibody (20 μg/ml) (Fukaya and Watanabe, 2000) or the mixture of rabbit anti-GluR1, -GluR2, and -GluR3 antibodies (20 μg/ml each) (Shimuta et al., 2001) overnight and colloidal gold (10 nm)-conjugated anti-rabbit IgG (British Biocell International, Cardiff, UK) for 2 h. They were stained with 2%

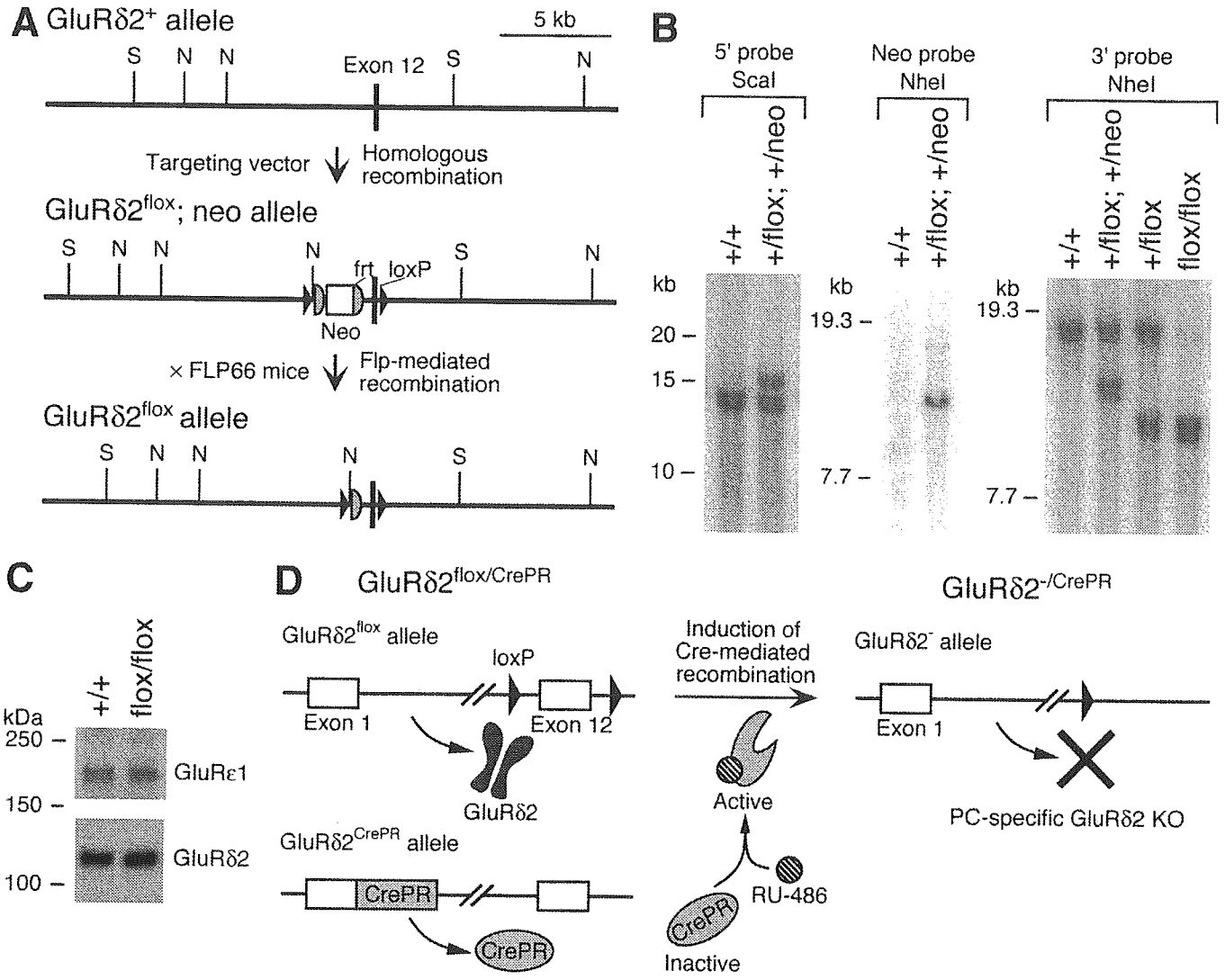

Figure 1. Inducible and PC-specific *GluRδ2* gene ablation by CrePR–loxP recombination system. ***A***, Schema of the exon 12 region of the *GluRδ2* gene (*GluRδ2*$^{+}$), floxed and *neo*-inserted allele (*GluRδ2*^{flox};*neo*), and floxed allele (*GluRδ2*^{flox}). Exon 12 encodes the putative transmembrane segment M3 of GluRδ2. The *GluRδ2*^{flox};*neo* allele contains two *loxP* sequences flanking exon 12 of the *GluRδ2* gene and the *neo* gene flanked by two *frt* sequences. The *neo* gene was removed *in vivo* by crossing *GluRδ2*$^{+/flox}$;+/*neo* mice with FLP66 mice carrying the Flp recombinase gene under the control of the *EF1α* promoter (Takeuchi et al., 2002). N, *Nhe*I; S, *Sca*I. ***B***, Southern blot analysis of genomic DNA from *GluRδ2*$^{+/+}$, *GluRδ2*$^{+/flox}$;+/*neo*, *GluRδ2*$^{+/flox}$, and *GluRδ2*$^{flox/flox}$ mice. Left, *Sca*I-digested DNA hybridized with 5′ probe; middle, *Nhe*I-digested DNA hybridized with neo probe; right, *Nhe*I-digested DNA hybridized with 3′ probe. ***C***, Western blot analysis of GluRδ2 and GluRε1 proteins in cerebellar homogenates from *GluRδ2*$^{+/+}$ and *GluRδ2*$^{flox/flox}$ mice. ***D***, Schema for induction of cerebellar PC-specific *GluRδ2* gene ablation in the adult brain. In *GluRδ2*$^{flox/CrePR}$ mice, one allele retains the intact *GluRδ2* gene with *loxP* sequences, and the other is inactivated by insertion of the *CrePR* gene. RU-486 administration induces recombination by CrePR, leading to *GluRδ2* gene knock-out in the adult brain in a cerebellar PC-specific manner.

uranyl acetate for 5 min and mixed lead solution for 30 s. The background level was defined as the density of immunogold particles fell within 30 nm on both sides from the mitochondrial membrane (GluRδ2 and AMPA receptors) or presynaptic nonjunctional membrane (PSD-93).

Statistical analysis. Data were analyzed by Student's *t* test or one-way ANOVA followed by Tukey–Kramer *post hoc* test.

Results

Inducible and cerebellar PC-specific GluRδ2 gene ablation

To address the functional roles of cerebellar PC-specific GluRδ2 in the adult brain by inducible Cre-mediated recombination, we constructed a targeting vector in which two *loxP* sequences were

→

Figure 2. Inducible and cerebellar PC-specific eliminations of *GluRδ2* mRNA and GluRδ2 proteins in *GluRδ2*$^{flox/CrePR}$ mice. We injected RU-486 into *GluRδ2*$^{flox/CrePR}$ mice at P42–P45 to induce CrePR recombinase activity. *GluRδ2*$^{flox/flox}$ mice injected with the antiprogestin served as controls. Temporal patterns of cerebellar PC-specific elimination of the *GluRδ2* mRNA and GluRδ2 proteins were assessed before and 2, 4, 8, 12, and 24 weeks after RU-486 treatment. ***A***, *In situ* hybridization analysis of the *GluRδ2* mRNA in the cerebella of *GluRδ2*$^{flox/flox}$ and *GluRδ2*$^{flox/CrePR}$ mice before and 2, 4, and 8 weeks after drug treatment. Parasagittal sections were hybridized with ^{33}P-labeled oligonucleotide probes and counterstained with methyl green-pyronine. Arrowheads indicate strongly labeled PCs. ***B***, Percentages of PCs labeled strongly for *GluRδ2* mRNA in the cerebella of *GluRδ2*$^{flox/flox}$ (○) and *GluRδ2*$^{flox/CrePR}$ (●) mice before and after drug treatment (2 mice). ***C***, Western blot analysis of GluRδ2 and GluRε1 proteins in the cerebella of *GluRδ2*$^{flox/flox}$ and *GluRδ2*$^{flox/CrePR}$ mice before and 4, 8, 12, and 24 weeks after drug treatment. ***D***, Relative expression levels of GluRδ2 proteins in the cerebella of *GluRδ2*$^{flox/flox}$ (○) and *GluRδ2*$^{flox/CrePR}$ (●) mice before and 4, 8, 12, and 24 weeks after RU-486 treatment (mean ± SEM; $n = 3$). A gray circle indicates the value of mock-treated *GluRδ2*$^{flox/CrePR}$ mice ($n = 3$). The amounts of GluRδ2 proteins in *GluRδ2*$^{flox/CrePR}$ mice before drug treatment were taken as 100%. ***E***, Immunohistochemical analysis of GluRδ2 proteins in the cerebella of *GluRδ2*$^{flox/flox}$ and *GluRδ2*$^{flox/CrePR}$ mice before and 4, 8, 12, and 24 weeks after drug treatment. ***F***, Cerebellar histology of *GluRδ2*$^{flox/flox}$ and *GluRδ2*$^{flox/CrePR}$ mice 8 weeks after RU-486 treatment. Shown are hematoxylin staining and immunofluorescence for calbindin (green) and GluRδ2 (red) in the molecular layer of the cerebellum. Scale bars: ***A***, 20 μm; ***E***, 1 mm; ***F***, 50 μm.

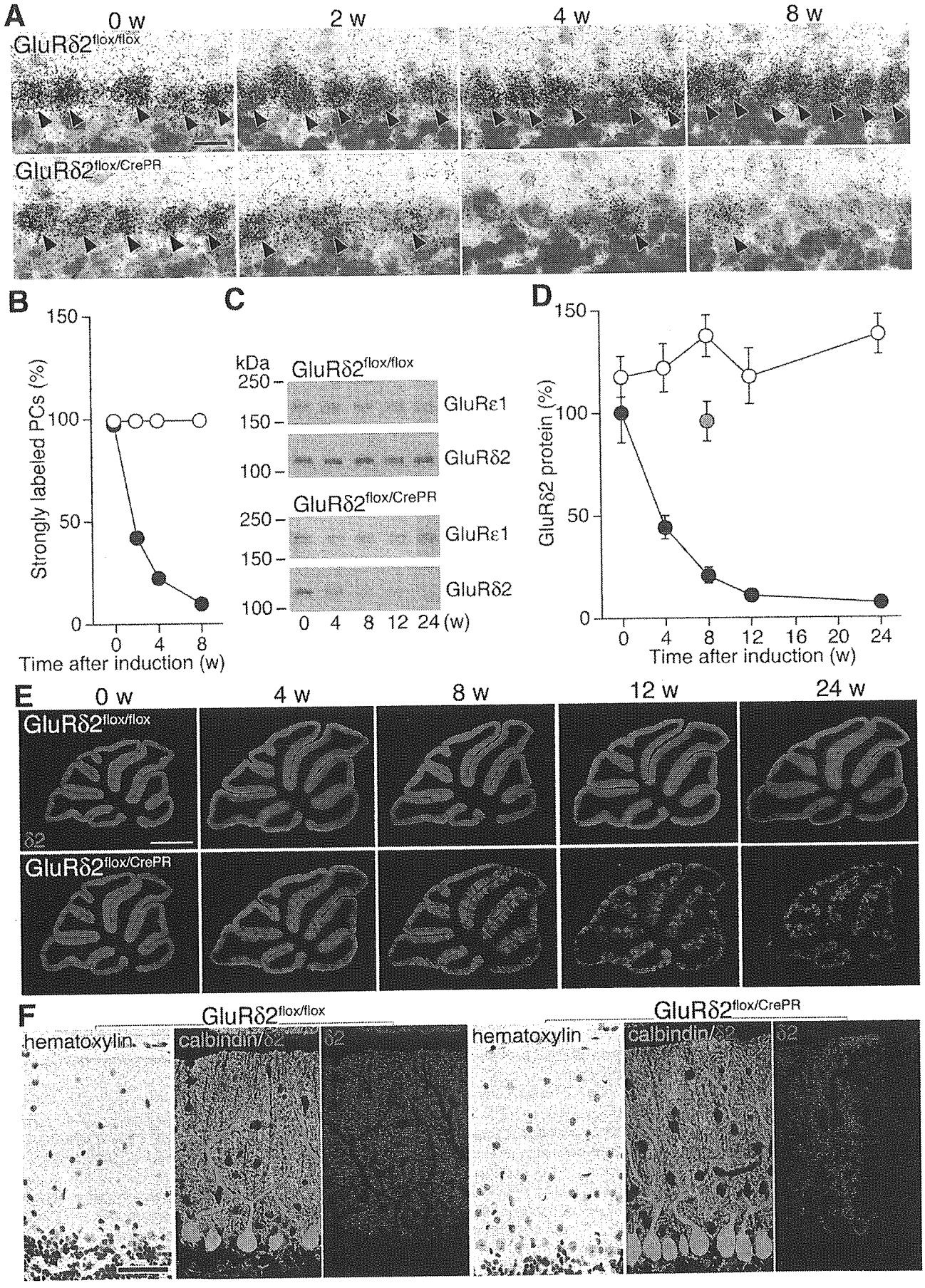
A
0 w
2 w
4 w
8 w
GluRδ2flox/flox
GluRδ2flox/CrePR
B
Strongly labeled PCs (%)
Time after induction (w)
C
kDa
GluRδ2flox/flox
GluRε1
GluRδ2
GluRδ2flox/CrePR
0 4 8 12 24 (w)
D
GluRδ2 protein (%)
Time after induction (w)
E
0 w
4 w
8 w
12 w
24 w
GluRδ2flox/flox
GluRδ2flox/CrePR
δ2
F
GluRδ2flox/flox
GluRδ2flox/CrePR
hematoxylin
calbindin/δ2
δ2

inserted into the mouse *GluRδ2* gene isolated from the C57BL/6 strain. The first *loxP* sequence linked to the *neo* gene flanked by two *frt* sites was in the intron upstream of exon 12 encoding putative transmembrane segment M3, and the second one was in the intron downstream of exon 12. Using a subline of ES cells derived from the C57BL/6 strain (Köntgen et al., 1993), we obtained recombinant $GluR\delta2^{+/flox}$;+/*neo* mice (Fig. 1*A*). By crossing to FLP66 transgenic mice of the C57BL/6 strain carrying an Flp recombinase expression vector under the control of the *EF1α* promoter (Takeuchi et al., 2002), we successfully eliminated the *neo* gene to yield $GluR\delta2^{+/flox}$ mice with the *GluRδ2* gene flanked by two *loxP* sequences (Fig. 1*B*). The expression of GluRδ2 proteins was comparable between $GluR\delta2^{+/+}$ and $GluR\delta2^{flox/flox}$ mice (Fig. 1*C*).

We crossed $GluR\delta2^{flox/flox}$ target mice with $GluR\delta2^{+/CrePR}$ mice carrying the *CrePR* gene inserted into the *GluRδ2* gene and thus were capable of mediating Cre–loxP recombination selectively in cerebellar PCs after induction (Kitayama et al., 2001). The resulting $GluR\delta2^{flox/CrePR}$ mice carrying the floxed *GluRδ2* gene on one allele and the *CrePR* gene on the other grew and mated normally. To examine the functional roles of GluRδ2 in the adult cerebellum, we induced the recombinase activity of CrePR by intraperitoneal injection of antiprogestin RU-486 into $GluR\delta2^{flox/CrePR}$ mice at P42–P45 for 2 consecutive days when cerebellar wiring was well completed and fully established PF–PC synapses were functional (Fig. 1*D*). $GluR\delta2^{flox/flox}$ mice treated with RU-486 served as controls. We first examined the expression of the *GluRδ2* mRNA in cerebellar PCs by *in situ* hybridization before and at 2, 4, and 8 weeks after RU-486 injection (Fig. 2*A*). Before antiprogestin administration, strong hybridization signals, defined as those with the signal-to-noise ratio >4.0, were found in almost all PCs of both $GluR\delta2^{flox/CrePR}$ (98%; $n = 2$) and $GluR\delta2^{flox/flox}$ (100%; $n = 2$) mice. RU-486 exerted little effect on the percentage of hybridization-positive PCs in $GluR\delta2^{flox/flox}$ mice (100% at 8 weeks after injection). In $GluR\delta2^{flox/CrePR}$ mice, however, the percentage of hybridization-positive PCs decreased to 23% at 4 weeks after RU-486 injection and gradually decreased thereafter with a reciprocal increase of PCs with low or no hybridization signals for the *GluRδ2* mRNA (Fig. 2*B*).

We then estimated the amounts of GluRδ2 proteins by immunoblot analysis, comparing those of NMDA receptor GluRε1 proteins that are expressed in cerebellar granule cells but not in PCs (Yamada et al., 2001) as internal standards (Fig. 2*C*,*D*). The amounts of GluRδ2 proteins in $GluR\delta2^{flox/flox}$ mice were essentially unaffected by RU-486 treatment. In contrast, GluRδ2 proteins gradually decreased to 21% at 8 weeks after RU-486 injection, indicating successful *GluRδ2* gene knock-out in mature PCs by the CrePR–antiprogestin induction system. $GluR\delta2^{flox/CrePR}$ mice at 8 weeks after mock treatment showed no decrease in the amount of GluRδ2 proteins (Fig. 2*D*). We further stained parasagittal cerebellar sections with anti-GluRδ2 antibody (Fig. 2*E*). Before induction, intense GluRδ2 immunoreactivity was present in the molecular layer of both $GluR\delta2^{flox/CrePR}$ and $GluR\delta2^{flox/flox}$ mice. RU-486 treatment of $GluR\delta2^{flox/flox}$ mice exerted little effect on GluRδ2 signals. In $GluR\delta2^{flox/CrePR}$ mice, however, A heterogeneous decrease of GluRδ2 immunoreactivity was discernable at 4 weeks after RU-486 injection. At 8 weeks, chimeric patterns of GluRδ2 signals became apparent with alternating strong and pale immunofluorescent bands in the molecular layer. At 12 weeks, pale or blank bands expanded in the molecular layer, being separated by thin bands with strong GluRδ2 immunoreactivity. The conditional ablation of GluRδ2 induced by RU-486 injection was not preferential in particular lobules or regions and occurred rather evenly in the anteroposterior and mediolateral axes of the cerebellum. Multiple factors may account for the relatively slow time course of GluRδ2 ablation. Knock-down of *GluRδ2* mRNA below the detection level in 80% of PCs took 4 weeks after administration of RU-486, suggesting a time lag between drug-induced activation of CrePR and mRNA degradation. Loss of 80% of GluRδ2 proteins took an additional 4 weeks, suggesting a slow turnover rate of GluRδ2 proteins.

The cerebellum of the RU-486-treated $GluR\delta2^{flox/CrePR}$ mice exhibited normal foliation and laminated cortical structures (Fig. 2*E*). No apparent differences were detectable in the thickness of the molecular and granular layers between $GluR\delta2^{flox/CrePR}$ and $GluR\delta2^{flox/flox}$ mice until 12 weeks after RU-486 treatment. Double immunostaining for GluRδ2 and calbindin revealed that PCs extended well arborized dendrites studded with numerous spines in $GluR\delta2^{flox/CrePR}$ and $GluR\delta2^{flox/flox}$ mice at 8 weeks after RU-486 treatment (Fig. 2*F*), indicating that the chimeric patterns of GluRδ2 immunoreactivity were not caused by the loss of PCs or distorted arborization of dendrites.

Appearance of synaptic mismatching and free spines

By electron microscopy, we inspected structures of PF–PC synapses in $GluR\delta2^{flox/CrePR}$ and $GluR\delta2^{flox/flox}$ mice at 8 weeks after RU-486 treatment; treated $GluR\delta2^{flox/CrePR}$ and $GluR\delta2^{flox/flox}$ mice were hereafter called mutant and control mice, respectively. Asymmetrical synapses were the most frequent type of synapses in the molecular layer of the cerebellum, and most of them were identified as PF–PC synapses on the basis of their characteristic morphology (Miyazaki et al., 2004). On single electron micrographs, all PC spines having PSD formed synaptic contacts with PFs in control mice (Fig. 3*A*). In mutant mice, however, some PC spines possessing PSD lacked presynaptic counterparts, suggesting the emergence of free spines (Fig. 3*B*, f). Furthermore, we noted that PSD in some contacted spines extended over the apposed active zone (Fig. 3*B*, arrows). In contrast, active zone and PSD were well matched in control mice (Fig. 3*A*).

We then examined randomly sampled PC spines by serial electron microscopy. In control mice, all PC spines had synaptic contacts with PF terminals (Fig. 3*C*). The analysis convincingly demonstrated the emergence of PC spines free from synaptic contacts in mutant mice, and they were thoroughly surrounded by cytoplasmic sheets of Bergmann glia (Fig. 3*D*). In such free spines, PSD-like condensation was present but was apparently smaller in size. These free spines were reminiscent of those found in *GluRδ2* null mutant mice (Kashiwabuchi et al., 1995; Kurihara et al., 1997).

Serial electron microscopy further enabled us to precisely classify PC spines of mutant mice as those forming matched contact, those forming mismatched contact, and free spines. For quantitative comparison, we defined a synapse as mismatched when the edges of the active zone and PSD were >100 nm apart in any of its serial sections. Under this criterion, almost all PC spines in control mice were classified as normal matched synapses [99.2 ± 0.6% (mean ± SEM); $n = 359$; three mice] (Fig. 3*E*). In contrast, 17.1 ± 3.3% of PC spines in mutant mice ($n = 358$; three mice) were free from synaptic contacts and 13.1 ± 2.7% had mismatched contacts with PF terminals (Fig. 3*G*,*H*). Such mismatching between the active zone and PSD was further confirmed by phosphotungstic acid cytochemistry that selectively visualizes electron-opaque materials in the active zone, synaptic cleft, and PSD (Bloom and Aghajanian, 1966) (Fig. 3*I–L*). Two-dimensional extents of the active zone and PSD were reconstructed from serial sections (Fig. 3*M–P*); when superimposed,

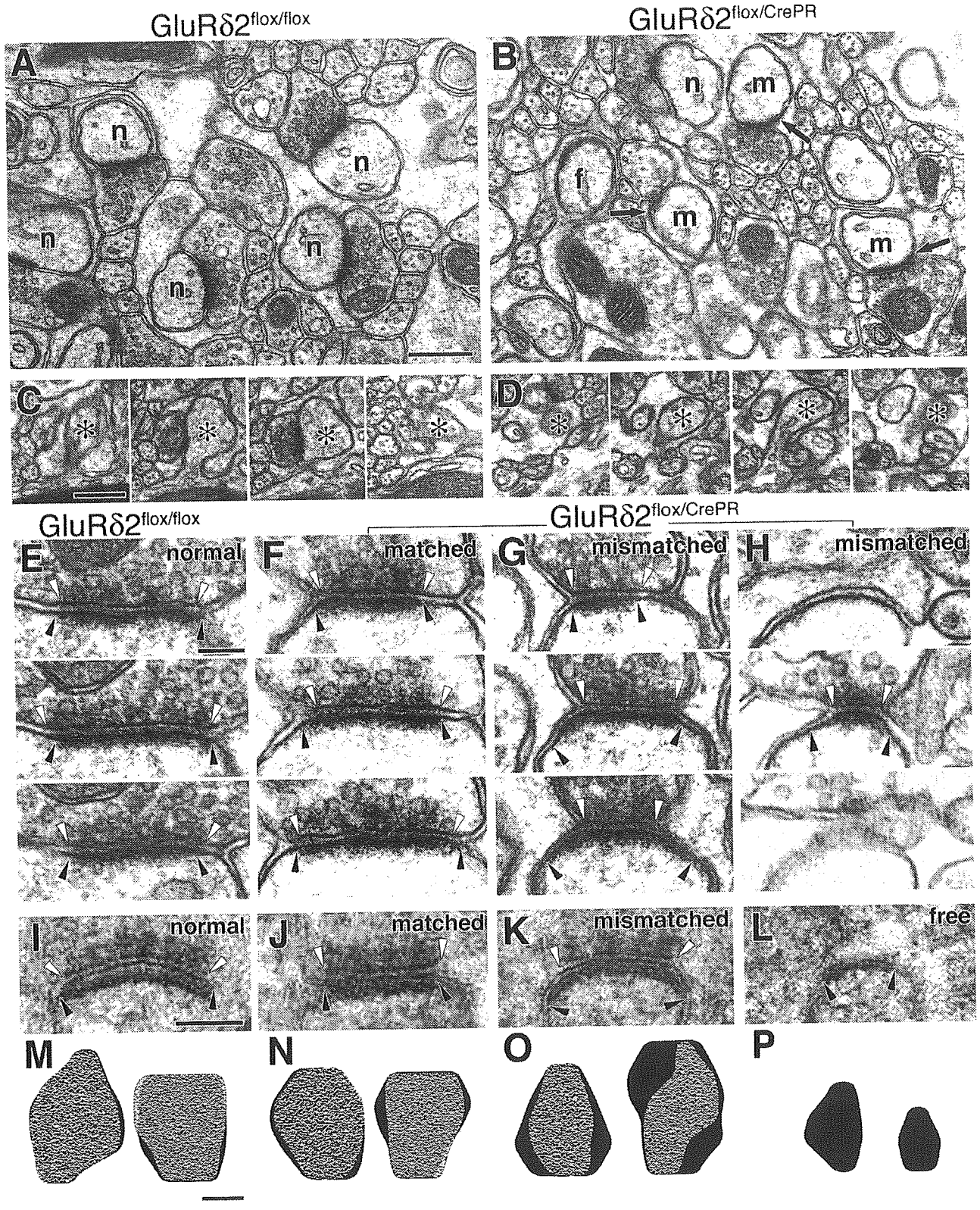

Figure 3. Emergence of mismatched PF–PC synapses and free PC spines. RU-486-treated *GluRδ2*$^{flox/flox}$ mice served as controls. ***A***, Normal synapses (n) in the cerebellum of a control mouse (RU-486-treated *GluRδ2*$^{flox/flox}$ mouse). Active zone and PSD are matched at all PF–PC synapses. ***B***, Mismatched synapses (m) and free spines (f) in the cerebellum of a mutant mouse (RU-486-treated *GluRδ2*$^{flox/CrePR}$ mouse). Arrows indicate the mismatch between active zone and PSD at PF–PC synapses. ***C***, ***D***, Serial images of a normal synapse in the control cerebellum (***C***) and of a free spine in the mutant cerebellum (***D***). Asterisks indicate dendritic spines of PCs. ***E–H***, Serial images through normal (***E***), matched (***F***), and mismatched (***G***, ***H***) synapses. White and black arrowheads indicate the edges of active zone and PSD, respectively. ***I–L***, Phosphotungstic acid cytochemistry of a normal synapse in the control cerebellum (***I***) and matched (***J***) and mismatched (***K***) synapses and a free spine (***L***) in the mutant cerebellum. White and black arrowheads indicate the edges of active zone and PSD, respectively. ***M–P***, Two-dimensionally reconstructed images of active zone (gray) and PSD (black) at normal (***M***), matched (***N***), and mismatched synapses (***O***), and free spines (***P***). Reconstruction was accomplished by stacking and smoothing images of three to six serial sections in the vertical axis. Linear outlines in the top and bottom sides are caused by the omission of sections through the margin of synapses, which were inappropriate for structural identification and reconstruction. Scale bars: ***A***, ***C***, 500 nm; ***E***, ***I***, ***M***, 200 nm.

these extents of the active zone and PSD overlapped at all synapses in control mice, thus being normal synapses (Fig. 3*M*). At mismatched synapses in mutant mice, PSD was irregularly expanded over the apposed active zone (Fig. 3*O*). Interestingly, some synapses classified as matched in mutant mice showed a dissociating tendency between active zone and PSD (Fig. 3*F,N*). Free spines had PSD, but the areas were smaller than those at normal, matched, and mismatched synapses (Fig. 3*P*). Free spines and mismatched synapses were hardly detectable in *GluRδ2*$^{flox/CrePR}$ mice at 8 weeks after mock treatment ($n = 300$; three mice).

Ablation of GluRδ2 proteins and structural alterations at PF–PC synapses

We applied postembedding immunogold to examine whether these structural alterations at PC synapses correlate with GluRδ2 protein levels at individual synapses. The labeling density per 1 μm of PSD length was determined by measuring the total number of gold particles and the total length of PSD appearing on serial sections through a given synapse (Fig. 4). The mean labeling density at normal synapses in control mice was 14.8 ± 0.9 ($n = 46$; three mice) (Fig. 4*A,E*). In mutant mice, the mean GluRδ2-labeling density decreased in the order of matched synapses (9.2 ± 0.7; $n = 65$; three mice) (Fig. 4*B,F*) > mismatched synapses (5.4 ± 0.6; $n = 44$) (Fig. 4*C,G*) > free spines (0.2 ± 0.2; $n = 18$) (Fig. 4*D,H*); the background density was 0.2 ± 0.1 ($n = 56$; total measured length, 116.4 μm). There were significant differences in the GluRδ2 labeling among matched synapses, mismatched synapses, and free spines in mutant mice (ANOVA, $F_{(2,124)} = 26.9$, $p < 0.0001$; *post hoc* test, $p < 0.01$). Furthermore, the GluRδ2-labeling density in the dissociated portion of PSD at mismatched synapses (1.2 ± 0.7; $n = 44$; three mice) was very low and close to that of free spines, whereas the density in the contacted portion at mismatched synapses (6.8 ± 0.7) was close to that of matched synapses. Thus, the density in the dissociated portion was much smaller than that in the contacted portion (*t* test; $p < 0.0001$).

Changes in sizes of the active zone and PSD

From serial profiles of a given classified synapse, we chose a single profile having the largest PSD to compare the length of active zone and PSD (45 synapses from three control mice; 43 matched and 39 mismatched synapses and 28 free spines from three mutant mice). As shown in Figure 5*A* by cumulative frequency plots, the length of active zone decreased significantly in the order of normal synapses in control mice (348 ± 12 nm) > matched synapses in mutant mice (296 ± 10 nm) > mismatched synapses in mutant mice (252 ± 10 nm) (ANOVA, $F_{(2,124)} = 19.1$, $p < 0.0001$; *post hoc* test, $p < 0.01$ for normal vs matched or mismatched; $p < 0.05$ for matched vs mismatched). Thus, the sizes of active zone corresponded well with the densities of GluRδ2 immunogold particles. The length of PSD decreased significantly in the order of normal synapses in control mice (379 ± 13 nm) > matched synapses in mutant mice (332 ± 10 nm) > free spines in mutant mice (226 ± 11 nm), but increased at mismatched synapses in mutant mice (424 ± 12 nm) (ANOVA, $F_{(3,151)} = 43.1$, $p < 0.0001$; *post hoc* test, $p < 0.01$ for normal vs free, matched vs mismatched or free, and mismatched vs free; $p < 0.05$ for normal vs matched or mismatched) (Fig. 5*B*). Consequently, the ratio of active zone to PSD lengths at mismatched synapses (0.59 ± 0.01) was significantly smaller than that at normal (0.92 ± 0.01) and matched synapses (0.89 ± 0.01) (ANOVA, $F_{(2,124)} = 167$, $p < 0.0001$; *post hoc* test, $p < 0.01$) (Fig. 5*C*).

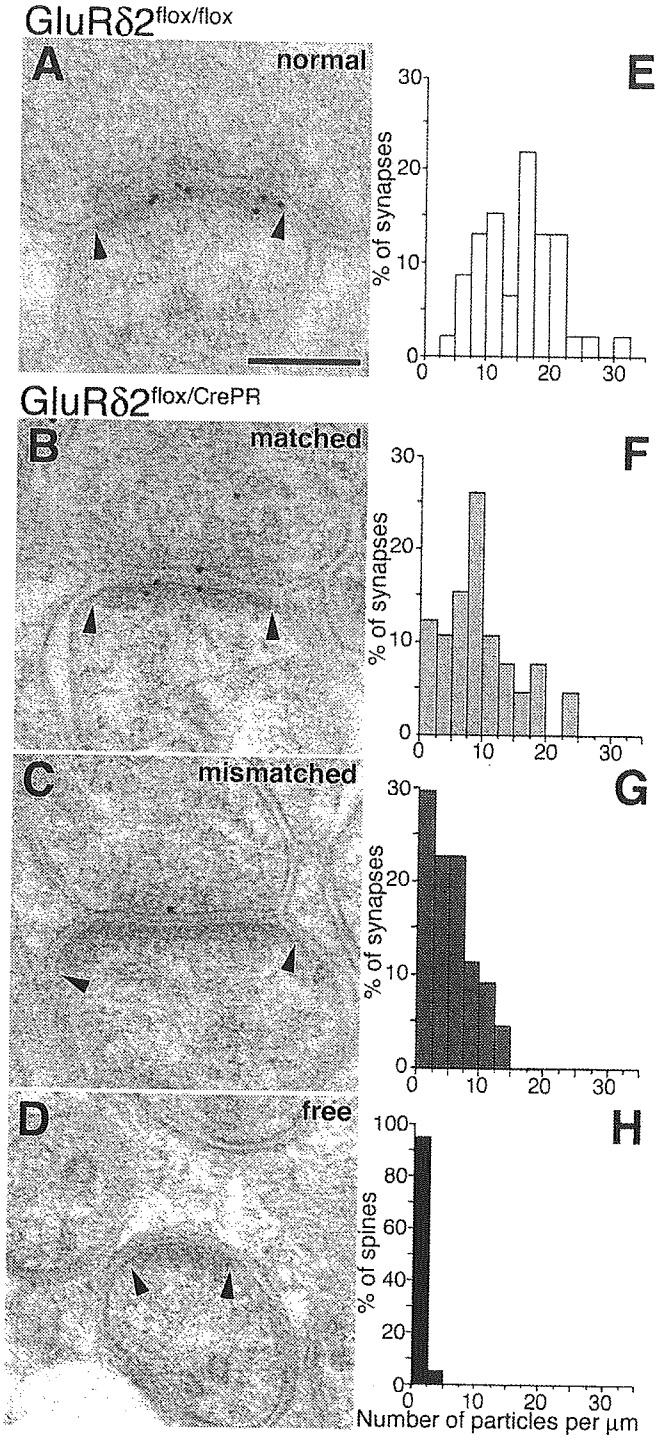

Figure 4. Immunogold electron microscopic analysis of GluRδ2 proteins. ***A–D***, Immunogold labeling for GluRδ2 proteins at a normal synapse in a control mouse (***A***) and at a matched synapse (***B***), a mismatched synapse (***C***), and a free spine (***D***) in a mutant mouse. Arrowheads indicate the edge of PSD. Scale bar, 200 nm. ***E–H***, Histograms for GluRδ2-labeling densities per 1 μm of PSD length at normal (***E***), matched synapses (***F***), mismatched synapses (***G***), and free spines (***H***). The number of labeled synapses was 46 of 46 for normal synapses, 60 of 65 for matched synapses, 41 of 44 for mismatched synapses, and 1 of 18 for free spines. Of the 41 labeled mismatched synapses, immunogold labeling at the contacted and dissociated portions was detected at 41 or 4 synapses, respectively.

Effect of GluRδ2 ablation on postsynaptic distributions of PSD-93 and AMPA receptor proteins

We further examined the effect of GluRδ2 ablation after the distribution of PSD-93 and AMPA receptors at PF–PC synapses

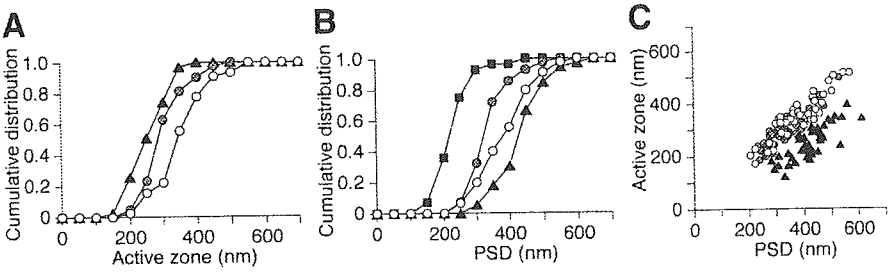

Figure 5. Lengths of the active zone and PSD. ***A***, ***B***, Cumulative frequency plots of active zone length (***A***) and PSD length (***B***) at normal synapses in control mice (open circles) and at matched synapses (filled circles), mismatched synapses (triangles), and free spines (squares) in mutant mice. ***C***, Scattergram plot between active zone and PSD lengths at normal (open circles), matched (filled circles), and mismatched synapses (triangles).

(Zhao et al., 1998; Roche et al., 1999; Fukaya and Watanabe, 2000) by postembedding immunogold. Because the labeling density for PSD-93 and AMPA receptors was much lower than that for GluRδ2, immunogold was applied to single sections, in which both sides of the sections are immunoreacted, thus leading to an increase in the sensitivity and accuracy of detection.

In mutant mice, the mean PSD-93-labeling density decreased in the order of matched synapses > mismatched synapses > free spines (Fig. 6*A*). There were significant differences in the PSD-93 labeling among matched synapses, mismatched synapses, and free spines in mutant mice (ANOVA, $F_{(2,429)} = 9.1$, $p = 0.0001$; *post hoc* test, $p < 0.05$ for matched vs mismatched; $p < 0.01$ for matched vs free). Furthermore, at mismatched synapses, the PSD-93-labeling density was higher in the contacted portion of PSD than in the dissociated portion (Fig. 6*B*), showing a significant difference (*t* test; $p = 0.03$).

PCs express high levels of AMPA receptor subunits, GluR1, GluR2, and GluR3 (Keinänen et al., 1990), and all of them are localized at PF synapses (Zhao et al., 1998). To further increase the labeling density of AMPA receptors, we used a mixture of antibodies against the GluR1, GluR2, and GluR3 subunits. In mutant mice, the mean AMPA receptor-labeling density decreased in the order of matched synapses > mismatched synapses > free spines (Fig. 6*C*). There were significant differences in the AMPA receptor labeling among matched synapses, mismatched synapses, and free spines in mutant mice (ANOVA, $F_{(2,407)} = 9.6$, $p < 0.0001$; *post hoc* test, $p < 0.01$ for matched vs mismatched or free). There were no significant differences in the AMPA receptor-labeling density between the contacted and dissociated portions of PSD at mismatched synapses (*t* test; $p = 0.10$) (Fig. 6*D*).

Temporal patterns of structural alterations at PF–PC synapses

We then examined the appearance of mismatched synapses and free spines in *GluRδ2*$^{flox/flox}$ and *GluRδ2*$^{flox/CrePR}$ mice before and at 4, 8, 12, and 24 weeks after RU-486 administration. Before antiprogestin treatment, there were very few, if any, free spines and mismatched synapses with PF terminals in both types of mice (Fig. 7*A*,*B*). After RU-486 administration, a significant number of mismatched synapses and free spines appeared at 4 weeks in *GluRδ2*$^{flox/CrePR}$ mice, and their fractions increased progressively toward 24 weeks (Fig. 7*E*). At 24 weeks, 42.0 ± 2.7% of PC spines ($n = 300$; three mice) were free from synaptic contacts with PFs and 28.3 ± 3.4% of spines had mismatched synapses, whereas matched synapses occupied only 29.7 ± 5.9% (Fig. 7*D*). On the other hand, free spines and mismatched synapses were very rare in antiprogestin-treated *GluRδ2*$^{flox/flox}$ mice even at 24 weeks after treatment (Fig. 7*C*).

Discussion

Neurobiological and behavioral traits are fairly complex and are most probably influenced by a large number of genes as well as environmental factors. There is ample evidence for large genetic differences between inbred mouse strains at the neurobiological and behavioral levels (Plomin, 1990; Wolfer et al., 1997). The inducible and neuron-specific gene targeting system developed in this study will be useful for dissecting the molecular basis of the structure and function of the adult brain under the pure C57BL/6 genetic background. Here we show that inducible ablation of GluRδ2 in the adult cerebellum resulted in mismatching between the active zone and PSD at PF–PC synapses. Furthermore, a significant number of PC spines became free from PF terminals. We thus identified GluRδ2 as a key molecule that regulates presynaptic and postsynaptic matching and synaptic connection in the adult brain. These results provide evidence for the notion that there is a common molecular mechanism underlying synaptic plasticity and synapse formation in the cerebellum (Kashiwabuchi et al., 1995). A number of molecules, including GluRs, receptor tyrosine kinases, and cell adhesion molecules, have been implicated in synapse formation and morphological maturation of dendritic spines during development (Hering and Sheng, 2001; Goda and Davis, 2003; Scheiffele, 2003), but the molecular basis of synaptic connection and its modulation in the adult brain are poorly understood. There is ample evidence for the involvement of NMDA receptors in synapse refinement *in vivo* during development and in structural modification of dendritic spines in cultured neurons (Goodman and Shatz, 1993; Engert and Bonhoeffer, 1999; Maletic-Savatic et al., 1999); however, no structural alterations were found at synapses by conditional ablation of NMDA receptors in the adult brain (Tsien et al., 1996; Rampon et al., 2000). In cultured hippocampal neurons, the AMPA receptor GluR2 subunit was important for morphogenesis of dendritic spines (Passafaro et al., 2003). On the other hand, no abnormalities in synaptic structures were detectable in mutant mice lacking the AMPA receptor GluR2 subunit (Sans et al., 2003; Petralia et al., 2004). Additional studies will be required to examine whether molecular determinants of synaptic structures during development are also important for modifications of synaptic structures in the adult brain. The present investigation provides direct evidence that GluRδ2 does regulate presynaptic and postsynaptic matching and synaptic connections in the adult cerebellum.

Immunogold labeling of GluRδ2 proteins under electron microscopy revealed that in mutant mice, the density of gold particles was reduced more at mismatched synapses than at matched synapses. Furthermore, the density of GluRδ2-labeling particles at mismatched synapses in mutant mice was much lower than that at normal synapses of control mice. Thus, certain amounts of GluRδ2 proteins in PSD are critical for proper matching of presynaptic and postsynaptic specializations. Consistently, GluRδ2-labeling particles were scarcely detectable in free PC spines of mutant mice. In addition, the fractions of mismatched synapses and free spines in total PC spines progressively increased concomitantly with the gradual decrease of GluRδ2 proteins after

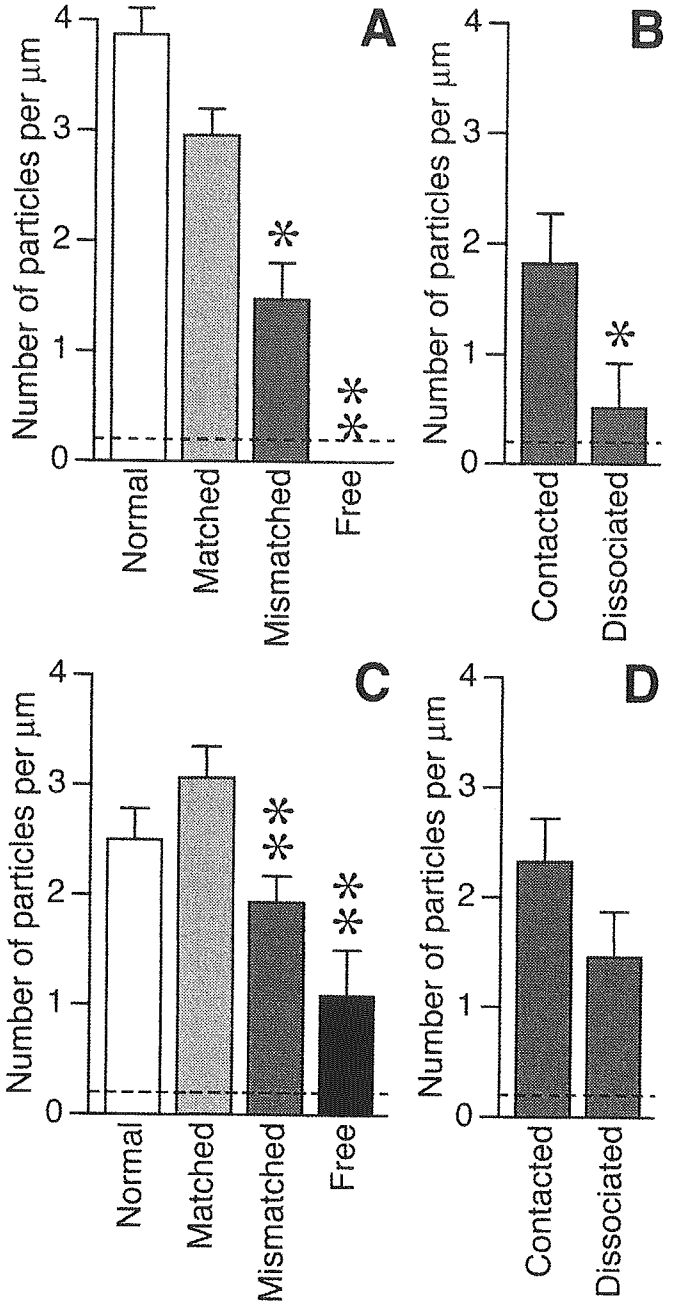

Figure 6. Immunogold electron microscopic analysis of PSD-93 and AMPA receptor proteins. ***A***, PSD-93-labeling densities per 1 μm of PSD length at normal synapses in three control mice and at matched synapses, mismatched synapses, and free spines in three mutant mice. The number of labeled synapses was 208 of 320 for normal synapses, 173 of 357 for matched synapses, 18 of 53 for mismatched synapses, and 0 of 22 for free spines. The background density was 0.2 ± 0.1 ($n = 53$; total measured length, 58.7 μm). ***B***, PSD-93-labeling densities in the contacted and dissociated portions of PSD at mismatched synapses in three mutant mice. Of the 18 labeled mismatched synapses, immunogold labeling at the contacted and dissociated portions was detected at 16 or 2 synapses, respectively. ***C***, AMPA receptor-labeling densities per 1 μm of PSD length at normal synapses in three control mice and at matched synapses, mismatched synapses, and free spines in three mutant mice. The number of labeled synapses was 98 of 225 for normal synapses, 121 of 231 for matched synapses, 64 of 123 for mismatched synapses, and 9 of 56 for free spines. The background density was 0.2 ± 0.1 ($n = 37$; total measured length, 36.8 μm). ***D***, AMPA receptor-labeling densities in the contacted and dissociated portions of PSD at mismatched synapses in three mutant mice. Of the 64 labeled mismatched synapses, immunogold labeling at the contacted and dissociated portions was detected at 53 or 15 synapses, respectively. Error bars represent SEM. Dotted lines indicate background densities. *$p < 0.05$; **$p < 0.01$.

antiprogestin induction of CrePR-mediated *GluRδ2* gene knockout in *GluRδ2*$^{flox/CrePR}$ mice. Thus, structural changes at PF–PC synapses appear to proceed from normal contacts via mismatched contacts to free spines according to the reduction of synaptic contents of GluRδ2 protein. As the density of GluRδ2 immunolabeling decreased, the length of the active zone became shorter in the order of normal, matched, and mismatched synapses. Furthermore, the dissociated portion of PSD at mismatched synapses showed a very low density of GluRδ2 immunogold particles such as free spines, whereas the density in the contacted portion at mismatched synapses was much higher and closer to that of matched synapses. The direct relationship between GluRδ2 density and synaptic contact suggests that postsynaptic GluRδ2 is essential for the maintenance of the presynaptic active zone and acts as the coordinator for presynaptic and postsynaptic differentiations. Thus, our results provide evidence for the postsynaptic control of the presynaptic active zone at mature synapses. Possibly, the postsynaptic GluRδ2 complex makes a physical linkage between the active zone and PSD to ensure the presynaptic and postsynaptic matching. There could be three potential mechanisms for this (supplemental Fig. 1, available at www.jneurosci.org as supplemental material). First, GluRδ2 may regulate the presynaptic active zone by direct interaction with an active zone component through its N-terminal domain. Interestingly, studies using cultured hippocampal neurons showed that an extracellular domain of the AMPA receptor GluR2 subunit was important for induction of dendritic spines (Passafaro et al., 2003). In addition, analysis of mutant mice showed that the laminin α4 chain that can bind to presynaptic Ca^{2+} channels was required for the apposition of active zones and junctional folds at the neuromuscular junction (Patton et al., 2001). Second, GluRδ2 may regulate the presynaptic active zone through the interaction between a postsynaptic GluRδ2-interacting molecule and an active zone component. Interestingly, NMDA-type GluRs interact with Eph receptor tyrosine kinases capable of *trans*-synaptic signaling (Dalva et al., 2000). In *Caenorhabditis elegans*, ionotropic glutamate receptor GLR-1 is colocalized at the cell surface with SOL-1 (suppressor of lurcher-1) containing four extracellular β-barrel-forming domains known as CUB (complement subcomponents C1r/C1s, Vegf, Bmp1) domains (Zheng et al., 2004). Third, GluRδ2 may regulate the presynaptic active zone more indirectly through a postsynaptic scaffold protein that binds to a molecule interacting with an active zone component. The C terminal of GluRδ2 associates with PSD-93 and PSD-95, which bind to the postsynaptic membrane protein neuroligin that is capable of interacting *trans*-synaptically with presynaptic β-neurexin (Roche et al., 1999; Kim and Sheng, 2004; Uemura et al., 2004); however, there were no detectable alterations in structures at PF–PC synapses in PSD-93 mutant mice (McGee et al., 2001). Multiple scaffold proteins might be functionally redundant. Thus, elucidation of the GluRδ2 mechanism will provide a key for understanding the regulation of synaptic connections in the adult brain and the precise topological matching of presynaptic and postsynaptic specializations that are essential for efficient synaptic transmission.

The length of PSD was significantly shorter at matched synapses in mutant mice than at normal synapses in control mice according to the significant decrease in the density of GluRδ2 immunogold particles at matched synapses in mutant mice. A further decrease in GluRδ2 proteins, however, resulted in enlargement of PSD at mismatched synapses compared with matched synapses in mutant mice. Namely, a strong decrease in GluRδ2 proteins at the postsynaptic site of PF–PC synapses

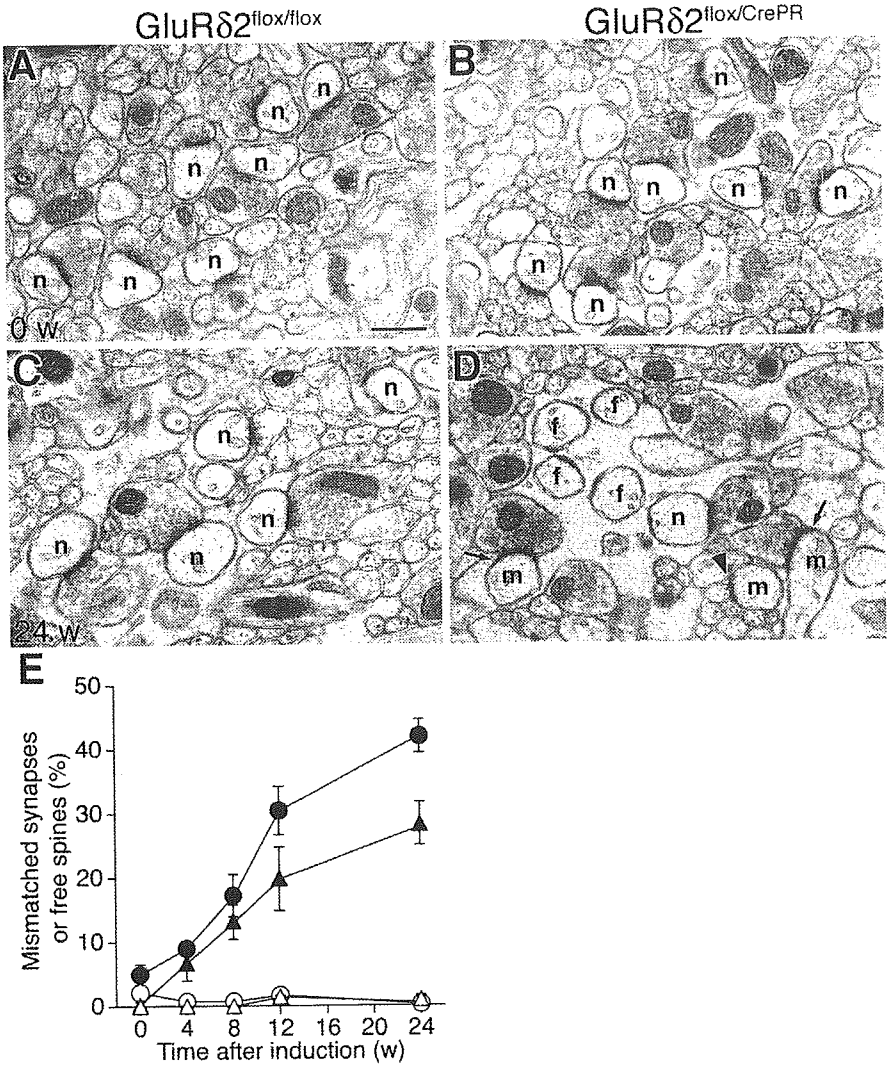

Figure 7. Temporal pattern of appearance of mismatched synapses and free spines in the cerebellum of *GluRδ2*$^{flox/CrePR}$ mice after CrePR induction by RU-486 treatment. RU-486-treated *GluRδ2*$^{flox/flox}$ mice served as controls. ***A–D***, Electron micrographs of PF–PC synapses in the cerebella of *GluRδ2*$^{flox/flox}$ (***A***, ***C***) and *GluRδ2*$^{flox/CrePR}$ (***B***, ***D***) mice before (***A***, ***B***) and 24 weeks after (***C***, ***D***) RU-486 treatment. Arrows indicate the mismatch between active zone and PSD at PF–PC synapses. An arrowhead indicates a rarely encountered abnormal spine, which possesses a PSD but contacts the nonterminal portion of PFs. f, Free spines; m, mismatched synapses; n, normal or matched synapses. Scale bar, 500 nm. ***E***, Percentages of mismatched synapses (triangles) and free spines (circles) in *GluRδ2*$^{flox/flox}$ and *GluRδ2*$^{flox/CrePR}$ mice before and 4, 8, 12, and 24 weeks after RU-486 treatment. Data from *GluRδ2*$^{flox/flox}$ and *GluRδ2*$^{flox/CrePR}$ mice are indicated by open and filled marks, respectively. Error bars represent SEM.

shrunk the active zone but increased the PSD. Thus, the opposite effect of GluRδ2 ablation on the sizes of the active zone and PSD caused mismatching between the presynaptic and postsynaptic differentiations. The C terminal of GluRδ2 associates with the PDZ (PSD-95/Discs large/zona occludens-1) domain-containing proteins, including PSD-93, protein tyrosine phosphatase PTP-MEG, and Delphilin (Roche et al., 1999; Hironaka et al., 2000; Miyagi et al., 2002). Recently, we found that GluRδ2 bound to the Shank family of scaffold proteins through an internal motif in the C-terminal region, and GluRδ2–Shank complexes associated with the metabotropic GluR1α, the AMPA-type GluR, and the inositol 1,4,5-trisphosphate receptor, which are essential for cerebellar long-term depression (Uemura et al., 2004). Thus, it is reasonable to assume that GluRδ2 regulates the organization of PSD through the interaction with multiple postsynaptic scaffold proteins. In fact, PSD-93 protein density decreased in parallel with the decrease of GluRδ2 proteins at PSD. Similar to GluRδ2 proteins, the PSD-93-labeling density was higher in the contacted portion of PSD than in the dissociated portion at mismatched synapses. On the other hand, there were no significant differences in the AMPA receptor-labeling density between the contacted and dissociated portions of PSD at mismatched synapses. In addition, AMPA receptor labeling was found in free spines without GluRδ2. The GluRδ2-linked distribution of PSD-93 and the relatively independent distribution of AMPA receptors at PSD suggest that GluRδ2 regulates the PSD organization at PF–PC synapses. Because ablation of PSD-93 alone appeared not to affect the synaptic structures (McGee et al., 2001), orchestration of multiple scaffold proteins by GluRδ2 may be essential. The decrease in GluRδ2 proteins at mismatched synapses thus caused the loosening of PSD organization, resulting in the enlargement of PSD. Loosening of PSD organization by GluRδ2 ablation may trigger the subsequent postsynaptic atrophy leading to free spines.

References

Araki K, Meguro H, Kushiya E, Takayama C, Inoue Y, Mishina M (1993) Selective expression of the glutamate receptor channel δ2 subunit in cerebellar Purkinje cells. Biochem Biophys Res Commun 197:1267–1276.

Bailey CH, Kandel ER (1993) Structural changes accompanying memory storage. Annu Rev Physiol 55:397–426.

Bloom FE, Aghajanian GK (1966) Cytochemistry of synapses: selective staining for electron microscopy. Science 154:1575–1577.

Dalva MB, Takasu MA, Lin MZ, Shamah SM, Hu L, Gale NW, Greenberg ME (2000) EphB receptors interact with NMDA receptors and regulate excitatory synapse formation. Cell 103:945–956.

Engert F, Bonhoeffer T (1999) Dendritic spine changes associated with hippocampal long-term synaptic plasticity. Nature 399:66–70.

Fukaya M, Watanabe M (2000) Improved immunohistochemical detection of postsynaptically located PSD-95/SAP90 protein family by protease section pretreatment: a study in the adult mouse brain. J Comp Neurol 426:572–586.

Funabiki K, Mishina M, Hirano T (1995) Retarded vestibular compensation in mutant mice deficient in δ2 glutamate receptor subunit. NeuroReport 7:189–192.

Goda Y, Davis GW (2003) Mechanisms of synapse assembly and disassembly. Neuron 40:243–264.

Goodman CS, Shatz CJ (1993) Developmental mechanisms that generate precise patterns of neuronal connectivity. Cell [Suppl] 72:77–98.

Hashimoto K, Ichikawa R, Takechi H, Inoue Y, Aiba A, Sakimura K, Mishina M, Hashikawa T, Konnerth A, Watanabe M, Kano M (2001) Roles of glutamate receptor δ2 subunit (GluRδ2) and metabotropic glutamate receptor subtype 1 (mGluR1) in climbing fiber synapse elimination during postnatal cerebellar development. J Neurosci 21:9701–9712.

Hering H, Sheng M (2001) Dendritic spines: structure, dynamics and regulation. Nat Rev Neurosci 2:880–888.

Hironaka K, Umemori H, Tezuka T, Mishina M, Yamamoto T (2000) The protein-tyrosine phosphatase PTPMEG interacts with glutamate receptor δ2 and ε subunits. J Biol Chem 275:16167–16173.

Ichikawa R, Miyazaki T, Kano M, Hashikawa T, Tatsumi H, Sakimura K,

Mishina M, Inoue Y, Watanabe M (2002) Distal extension of climbing fiber territory and multiple innervation caused by aberrant wiring to adjacent spiny branchlets in cerebellar Purkinje cells lacking glutamate receptor δ2. J Neurosci 22:8487–8503.

Kashiwabuchi N, Ikeda K, Araki K, Hirano T, Shibuki K, Takayama C, Inoue Y, Kutsuwada T, Yagi T, Kang Y, Aizawa S, Mishina M (1995) Impairment of motor coordination, Purkinje cell synapse formation, and cerebellar long-term depression in GluRδ2 mutant mice. Cell 81:245–252.

Keinänen K, Wisden W, Sommer B, Werner P, Herb A, Verdoorn TA, Sakmann B, Seeburg PH (1990) A family of AMPA-selective glutamate receptors. Science 249:556–560.

Kim E, Sheng M (2004) PDZ domain proteins of synapses. Nat Rev Neurosci 5:771–781.

Kishimoto Y, Kawahara S, Suzuki M, Mori H, Mishina M, Kirino Y (2001) Classical eyeblink conditioning in glutamate receptor subunit δ2 mutant mice is impaired in the delay paradigm but not in the trace paradigm. Eur J Neurosci 13:1249–1253.

Kitayama K, Abe M, Kakizaki T, Honma D, Natsume R, Fukaya M, Watanabe M, Miyazaki J, Mishina M, Sakimura K (2001) Purkinje cell-specific and inducible gene recombination system generated from C57BL/6 mouse ES cells. Biochem Biophys Res Commun 281:1134–1140.

Köntgen F, Süss G, Stewart C, Steinmetz M, Bluethmann H (1993) Targeted disruption of the MHC class II *Aa* gene in C57BL/6 mice. Int Immunol 5:957–964.

Kurihara H, Hashimoto K, Kano M, Takayama C, Sakimura K, Mishina M, Inoue Y, Watanabe M (1997) Impaired parallel fiber-Purkinje cell synapse stabilization during cerebellar development of mutant mice lacking the glutamate receptor δ2 subunit. J Neurosci 17:9613–9623.

Lalouette A, Lohof A, Sotelo C, Guénet J-L, Mariani J (2001) Neurobiological effects of a null mutation depend on genetic context: comparison between two hotfoot alleles of the delta-2 ionotropic glutamate receptor. Neuroscience 105:443–455.

Lamprecht R, LeDoux J (2004) Structural plasticity and memory. Nat Rev Neurosci 5:45–54.

Landsend AS, Amiry-Moghaddam M, Matsubara A, Bergersen L, Usami S, Wenthold RJ, Ottersen OP (1997) Differential localization of δ glutamate receptors in the rat cerebellum: coexpression with AMPA receptors in parallel fiber-spine synapses and absence from climbing fiber-spine synapses. J Neurosci 17:834–842.

Lomeli H, Sprengel R, Laurie DJ, Köhr G, Herb A, Seeburg PH, Wisden W (1993) The rat delta-1 and delta-2 subunits extend the excitatory amino acid receptor family. FEBS Lett 315:318–322.

Maletic-Savatic M, Malinow R, Svoboda K (1999) Rapid dendritic morphogenesis in CA1 hippocampal dendrites induced by synaptic activity. Science 283:1923–1927.

Martin SJ, Grimwood PD, Morris RGM (2000) Synaptic plasticity and memory: an evaluation of the hypothesis. Annu Rev Neurosci 23:649–711.

McGee AW, Topinka JR, Hashimoto K, Petralia RS, Kakizawa S, Kauer FW, Aguilera-Moreno A, Wenthold RJ, Kano M, Bredt DS (2001) PSD-93 knock-out mice reveal that neuronal MAGUKs are not required for development or function of parallel fiber synapses in cerebellum. J Neurosci 21:3085–3091.

Mishina M (2003) Timing determines the neural substrates for eyeblink conditioning. Int Congr Ser 1250:473–486.

Miyagi Y, Yamashita T, Fukaya M, Sonoda T, Okuno T, Yamada K, Watanabe M, Nagashima Y, Aoki I, Okuda K, Mishina M, Kawamoto S (2002) Delphilin: a novel PDZ and formin homology domain-containing protein that synaptically colocalizes and interacts with glutamate receptor δ2 subunit. J Neurosci 22:803–814.

Miyazaki T, Hashimoto K, Shin H-S, Kano M, Watanabe M (2004) P/Q-type Ca^{2+} channel αlA regulates synaptic competition on developing cerebellar Purkinje cells. J Neurosci 24:1734–1743.

Nakagawa S, Watanabe M, Isobe T, Kondo H, Inoue Y (1998) Cytological compartmentalization in the staggerer cerebellum, as revealed by calbindin immunohistochemistry for Purkinje cells. J Comp Neurol 395:112–120.

Passafaro M, Nakagawa T, Sala C, Sheng M (2003) Induction of dendritic spines by an extracellular domain of AMPA receptor subunit GluR2. Nature 424:677–681.

Patton BL, Cunningham JM, Thyboll J, Kortesmaa J, Westerblad H, Edström L, Tryggvason K, Sanes JR (2001) Properly formed but improperly localized synaptic specializations in the absence of laminin α4. Nat Neurosci 4:597–604.

Petralia RS, Sans N, Wang Y-X, Vissel B, Chang K, Noben-Trauth K, Heinemann SF, Wenthold RJ (2004) Loss of GluR2 α-amino-3-hydroxy-5-methyl-4-isoxazoleproprionic acid receptor subunit differentially affects remaining synaptic glutamate receptors in cerebellum and cochlear nuclei. Eur J Neurosci 19:2017–2029.

Plomin R (1990) The role of inheritance in behavior. Science 248:183–188.

Rampon C, Tang Y-P, Goodhouse J, Shimizu E, Kyin M, Tsien JZ (2000) Enrichment induces structural changes and recovery from nonspatial memory deficits in CA1 NMDAR1-knockout mice. Nat Neurosci 3:238–244.

Roche KW, Ly CD, Petralia RS, Wang Y-X, McGee AW, Bredt DS, Wenthold RJ (1999) Postsynaptic density-93 interacts with the δ2 glutamate receptor subunit at parallel fiber synapses. J Neurosci 19:3926–3934.

Sans N, Vissel B, Petralia RS, Wang Y-X, Chang K, Royle GA, Wang C-Y, O'Gorman S, Heinemann SF, Wenthold RJ (2003) Aberrant formation of glutamate receptor complexes in hippocampal neurons of mice lacking the GluR2 AMPA receptor subunit. J Neurosci 23:9367–9373.

Scheiffele P (2003) Cell-cell signaling during synapse formation in the CNS. Annu Rev Neurosci 26:485–508.

Shimuta M, Yoshikawa M, Fukaya M, Watanabe M, Takeshima H, Manabe T (2001) Postsynaptic modulation of AMPA receptor-mediated synaptic responses and LTP by the type 3 ryanodine receptor. Mol Cell Neurosci 17:921–930.

Takayama C, Nakagawa S, Watanabe M, Mishina M, Inoue Y (1996) Developmental changes in expression and distribution of the glutamate receptor channel δ2 subunit according to the Purkinje cell maturation. Brain Res Dev Brain Res 92:147–155.

Takeuchi T, Nomura T, Tsujita M, Suzuki M, Fuse T, Mori H, Mishina M (2002) Flp recombinase transgenic mice of C57BL/6 strain for conditional gene targeting. Biochem Biophys Res Commun 293:953–957.

Taniguchi M, Yuasa S, Fujisawa H, Naruse I, Saga S, Mishina M, Yagi T (1997) Disruption of *semaphorin III/D* gene causes severe abnormality in peripheral nerve projection. Neuron 19:519–530.

Tsien JZ, Huerta PT, Tonegawa S (1996) The essential role of hippocampal CA1 NMDA receptor-dependent synaptic plasticity in spatial memory. Cell 87:1327–1338.

Tsujita M, Mori H, Watanabe M, Suzuki M, Miyazaki J, Mishina M (1999) Cerebellar granule cell-specific and inducible expression of Cre recombinase in the mouse. J Neurosci 19:10318–10323.

Uemura T, Mori H, Mishina M (2004) Direct interaction of GluRδ2 with Shank scaffold proteins in cerebellar Purkinje cells. Mol Cell Neurosci 26:330–341.

Watanabe M, Inoue Y, Sakimura K, Mishina M (1993) Distinct distributions of five *N*-methyl-D-aspartate receptor channel subunit mRNAs in the forebrain. J Comp Neurol 338:377–390.

Watanabe M, Fukaya M, Sakimura K, Manabe T, Mishina M, Inoue Y (1998) Selective scarcity of NMDA receptor channel subunits in the stratum lucidum (mossy fibre-recipient layer) of the mouse hippocampal CA3 subfield. Eur J Neurosci 10:478–487.

Wolfer DP, Müller U, Stagliar M, Lipp H-P (1997) Assessing the effects of the 129/Sv genetic background on swimming navigation learning in transgenic mutants: a study using mice with a modified β-amyloid precursor protein gene. Brain Res 771:1–13.

Yamada K, Fukaya M, Shimizu H, Sakimura K, Watanabe M (2001) NMDA receptor subunits GluRε1, GluRε3 and GluRζ1 are enriched at the mossy fibre-granule cell synapse in the adult mouse cerebellum. Eur J Neurosci 13:2025–2036.

Yamazaki M, Araki K, Shibata A, Mishina M (1992) Molecular cloning of a cDNA encoding a novel member of the mouse glutamate receptor channel family. Biochem Biophys Res Commun 183:886–892.

Zhao H-M, Wenthold RJ, Petralia RS (1998) Glutamate receptor targeting to synaptic populations on Purkinje cells is developmentally regulated. J Neurosci 18:5517–5528.

Zheng Y, Mellem JE, Brockie PJ, Madsen DM, Maricq AV (2004) SOL-1 is a CUB-domain protein required for GLR-1 glutamate receptor function in *C. elegans*. Nature 427:451–457.

Case Report

A clinical trial of ribavirin administration for Japanese encephalitis : a case report

Takaaki Tokito[1], Morihiro Tajiri[1], Mitsuyoshi Ayabe[1], Hiroshi Shoji[1]*, Yasuhiko Maeyama[2] and Nobuyuki Hirohashi[2]

Abstract : We report herein a trial of ribavirin administration for a case of Japanese encephalitis (JE). A 69-year-old female developed acute encephalitis at the end of September 2003, and the diagnosis of JE was serologically confirmed. Ribavirin at 400 mg per day was periorally given starting with the 11th illness day. Despite ribavirin administration for 2 weeks, the patient lapsed into a vegetative state. Our report suggests that ribavirin therapy, possibly combined with interferon-α, for JE should be initiated at the earliest possible time.

(Neuroinfection, 10 : 94—97, 2005)

Key words : flavivirus, Japanese encephalitis, ribavirin, Russian Spring-Summer encephalitis, West Nile encephalitis

Introduction

Japanese encephalitis (JE) is known to have poor outcomes with an approximately 30% mortality rate. In Japan, the number of JE cases has decreased to several patients per year due to JE vaccination of children and the decreased number of pig farms located near cities. It should also be noted that the occurrence of JE appears to have shifted from September to October. A megatrial of interferon-α (IFN-α) for 112 Vietnamese children with JE[1] has been reported. We report herein a clinical trial of ribavirin for an elderly patient with JE.

Case report

A 69-year-old woman who had no certain mosquito bites experienced an acute onset with fever and a confusional state at the end of September 2003 (Fig. 1). On September 29, the patient was admitted to our University Hospital, and she showed a coma state with meningeal irritation signs. The cerebrospinal fluid (CSF) revealed moderate pleocytosis (213/μl), protein 163 mg/dl, and normal glucose levels. Plain computed tomography (CT) of the brain on the 3rd illness day revealed no abnormalities. An electroencephalogram (EEG) revealed periodic synchronous discharges. The patient was treated with acyclovir at 1.5 g per day due to our suspicion of herpes simplex encephalitis (HSE). Four days after the first CT examination, magnetic resonance imaging (MRI) of the brain demonstrated high signal intensities in the bilateral thalami, basal ganglia, hippocampi, and brainstem, including the substantia nigra (Fig. 2). JE was strongly suspected on basis of the bilateral MRI abnormalities in the thalamic lesions, including the substantia nigra.

A ribavirin therapy plan for JE was submitted to the Kurume University ethical committee, and informed consent for the ribavirin therapy was gained from the patient's family. At the 11th illness day, ribavirin was periorally started at 400 mg per day, and was continued for 2 weeks. This treat-

[1] First Department of Internal Medicine, [2] Department of Emergency and Critical Care Medicine, Kurume University School of Medicine (Asahimachi 67, Kurume 830-0011, Japan)

Received January 10, 2005 ; accepted February 21, 2005. Corresponding author (e-mail : hshoji@med.kurume-u.ac.jp)

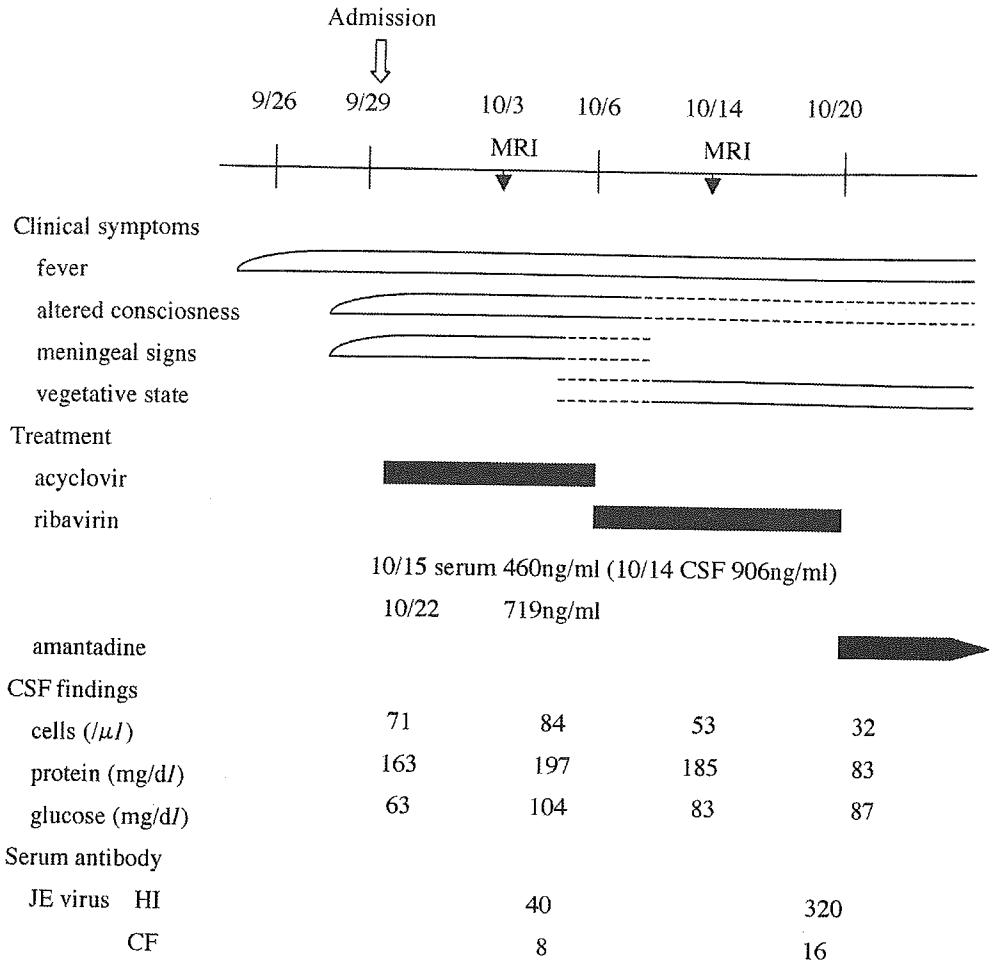

Fig. 1 Clinical course

MRI : magnetic resonance imaging ; CSF : cerebrospinal fluid ; JE : Japanese encephalitis ; CF : complement fixation ; HI : hemagglutination inhibition

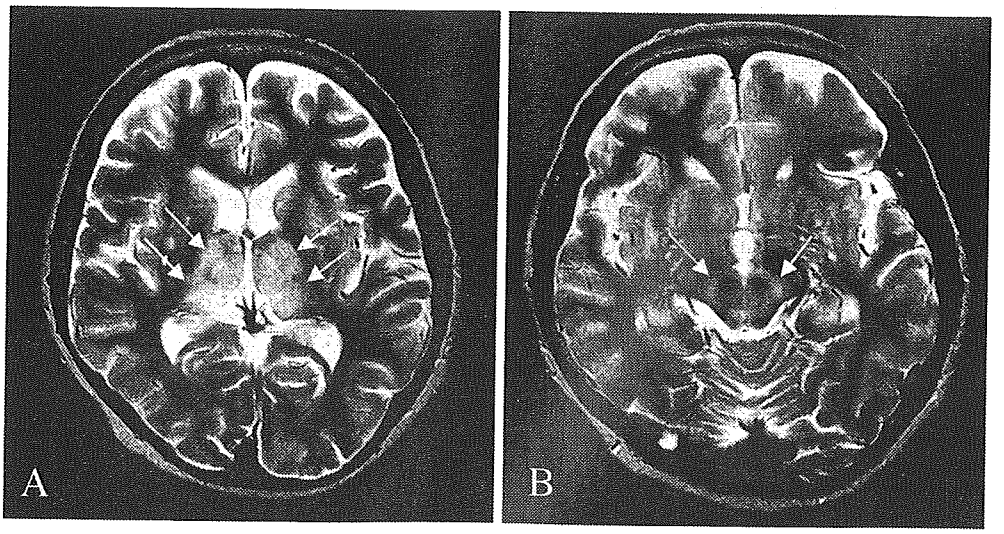

Fig. 2 MRIs of Japanese encephalitis.

One week after onset, T2-weighted axial MRI images revealing high signal lesions bilaterally in the thalami (A, arrows), basal ganglia, and substantia nigra (B, arrows).

ment was followed by administration of amantadine at 150 mg per day for 2 weeks, which was used to treat the patient's severe cognitive impairment rather than for its use of antiviral activity. The serum levels of ribavirin were 460 ng/μl, while the CSF levels were rather high at 906 ng/μl. Significant increases in complement fixation and hemagglutination inhibition titers for JE virus were confirmed from acute to recovery stages. Changes in consciousness levels, neurological symptoms, and laboratory data were evaluated as efficacy markers of ribavirin therapy. The CSF cells and protein level were improved. However, 2 months later, severe dementia, involuntary movement, and tetraparesis remained. Mild anemia was noted as a side effect of the ribavirin therapy in our case.

Discussion

In vitro studies have shown the antiviral activity of IFN-α, ribavirin, 6-azauridine, and gycyrrhizin against JE virus and other flaviviruses[2][3]. Solomon et al[1] conducted a randomized double-blind placebo-controlled trial of IFN-α-2a in 112 Vietnamese children with JE. Their results did not show improved the outcomes for patients with JE, and they indicated that a combined therapy of IFN-α-2a and ribavirin should be considered. Our patient continued to survive at 3 months after the onset, but the patient had lapsed into a vegetative state; her severe sequelae may have been caused by the delayed administration. In future, the optimal doses of ribavirin or a combined therapy with IFN-α should be investigated. Meanwhile, the efficacy of ribavirin treatment for 140 patients with acute Nipah encephalitis caused by a new paramyxovirus[4] has been reported ; a 36% reduction in mortality was observed, though it was an open trial. On the other hand, when intraventricular ribavirin and IFN-α combination therapy was conducted for 10 patients with subacute sclerosing panencephalitis (SSPE)[5], some patients showed clinical improvement, though mild side effects such as lip swelling, sleepiness and headache were noted.

In Japan, a problem has arisen with regard to the early administration of antiviral therapy against JE; in recent years, the number of JE cases has decreased to several patients per year, and the onset time has sometimes shifted to the end of September to even October, as shown in this case and in reports from other districts in Japan[6][7]. Accordingly, JE is treated as an acute sporadic encephalitis such as HSE.

In our case, acyclovir was initiated due to our suspicion of HSE based on the presence of periodic synchronous discharges on EEG. Ribavirin therapy was then started as soon as the characteristic MRI findings appeared[8]. For patients with acute encephalitis presenting MRI abnormalities in the bilateral thalamic, including the substantia nigra, our report suggests that JE should be considered as a possible differential diagnosis, and treatment with ribavirin alone or with IFN-α combined administration should be considered instead of acyclovir therapy.

Finally, MRI changes are also observed in other flavivirus encephalitides such as Russian Spring-Summer encephalitis, Murrey Valley encephalitis, West Nile encephalitis, and St. Louis encephalitis[9][10]. Unfortunately, it is possible that these encephalitides could occur in Japan in the near future. Accordingly, MRI findings may be a useful tool for early diagnosis, making possible early antiviral therapy.

References

1) Solomon T, Dung NM, Wills B, et al : Interferon alfa-2a in Japanese encephalitis : a randomised double-blind placebo-controlled trial. Lancet 361 : 821—826, 2003.

2) Crance JM, Scaramozzino N, Jouan A, et al : Interferon, ribavirin, 6-azauridine and glycyrrhizin : antiviral compounds active against pathogenic flaviviruses. Antiviral Res 58 : 73—79, 2003.

3) Morrey JD, Day CW, Julander JG, et al : Effect of interferon-alpha and interferon-inducers on West Nile virus in mouse and hamster animal models. Antivir Chem Chemother 15 : 101—109, 2004.

4) Chong HT, Kamarulzaman A, Tan CT, et al : Treatment of acute Nipah encephalitis with ribavirin. Ann Neurol 49 : 810—813, 2001.

5) Tomoda A, Nomura K, Shiraishi S, et al : Trial of intraventicular ribavirin and interferon-alfa combination therapy for subacute sclerosing panencephalitis (SSPE) in